

Review

Hierarchically Porous Vanadium-Based Cathode Materials for High-Performance Na-Ion Batteries

Kanakaraj Aruchamy ^{1,2,†}, Subramaniyan Ramasundaram ^{1,†}, Athinarayanan Balasankar ³,
Sivasubramani Divya ¹, Ling Fei ^{2,*} and Tae Hwan Oh ^{1,*}

¹ School of Chemical Engineering, Yeungnam University, Gyeongsan 38541, Republic of Korea; a.kanakaraj@yu.ac.kr (K.A.); ramasundaram79@hotmail.com (S.R.); divi.fysics@gmail.com (S.D.)

² Department of Chemical Engineering, University of Louisiana at Lafayette, Lafayette, LA 70504, USA

³ Department of Physics, Gobi Arts & Science College, Gobichettipalayam, Erode 638453, Tamilnadu, India; balphd1987@gmail.com

* Correspondence: ling.fei@louisiana.edu (L.F.); taehwano@ynu.ac.kr (T.H.O.)

† These authors contributed equally to this work.

Abstract: Sodium-ion batteries (SIBs) have emerged as a promising alternative to lithium-ion batteries (LIBs) in sectors requiring extensive energy storage. The abundant availability of sodium at a low cost addresses concerns associated with lithium, such as environmental contamination and limited availability. However, SIBs exhibit lower energy density and cyclic stability compared to LIBs. One of the key challenges in improving the performance of SIBs lies in the electrochemical properties of the cathode materials. Among the various cathodes utilized in SIBs, sodium vanadium phosphates (NVPs) and sodium vanadium fluorophosphates (NVPFs) are particularly advantageous. These vanadium-based cathodes offer high theoretical capacity and are cost-effective. Commercialization of SIBs with NVPF cathodes has already begun. However, the poor conductivity of these cathode materials leads to a short cycle life and inferior rate performance. Various synthesis methods have been explored to enhance the conductivity, including heteroatom doping (N, S, and Co), surface modification, the fabrication of porous nanostructures, and composite formation with conductive carbon materials. In particular, cathodes with interconnected hierarchical micro- and nano-porous morphologies have shown promise. This review focuses on the diverse synthesis methods reported for preparing hierarchically porous cathodes. With increased attention, particular emphasis has been placed on carbon composites of NVPs and NVPFs. Additionally, the synthesis of vanadium pentoxide-based cathodes is also discussed.

Keywords: hierarchical structures; porous materials; cathodes; Na-ion batteries



Citation: Aruchamy, K.; Ramasundaram, S.; Balasankar, A.; Divya, S.; Fei, L.; Oh, T.H. Hierarchically Porous Vanadium-Based Cathode Materials for High-Performance Na-Ion Batteries. *Batteries* **2024**, *10*, 223. <https://doi.org/10.3390/batteries10070223>

Academic Editor: Yu Jiang

Received: 9 May 2024

Revised: 13 June 2024

Accepted: 21 June 2024

Published: 24 June 2024



Copyright: © 2024 by the authors. Licensee MDPI, Basel, Switzerland. This article is an open access article distributed under the terms and conditions of the Creative Commons Attribution (CC BY) license (<https://creativecommons.org/licenses/by/4.0/>).

1. Introduction

Sodium-ion batteries (SIBs) and lithium-ion batteries (LIBs) were developed concurrently during the same period in the 1980s. Both belong to the category of alkaline metals and share similarities in their atomic properties, ionicity, electronegativity, and electrochemical behavior. However, in recent years, SIBs have garnered increased attention due to the high cost and limitations associated with the predominant energy storage device, LIBs. In terms of battery application and operation, the chemistry of SIBs and LIBs exhibits notable similarities [1–4]. Limited lithium resources, stringent environmental regulations, and the absence of effective Li-recycling technology have posed significant obstacles to the widespread adoption of LIBs. In contrast, the abundance, low cost, inexhaustible availability on Earth, and easy accessibility of sodium serve as key advantages that drive the widespread application of SIBs [4–7]. SIBs have demonstrated the capability to store energy on a par with certain commercial LIBs, presenting a promising alternative derived from naturally abundant and cost-effective sodium. The abundance of lithium and sodium in the Earth's crust is estimated to be 23,600 and 20 parts per million (ppm), respectively,

with sodium's extraction costs being lower than those of lithium. Moreover, metal oxides containing sodium and polyanion cathodes can be derived from transition metals (such as Fe, Mn, V, and Ti), which are plentiful in nature. Therefore, SIBs are anticipated to be economically feasible in both affluent and economically disadvantaged regions. In the case of lithium-powered vehicles, it is estimated that 40–60% of the total cost is attributed to batteries, with lithium carbonate accounting for 10–15% of the battery cost. This shows the urgent need for sustainable and transformative solutions. Anticipated breakthroughs in SIB-based energy storage applications are expected to substantially reduce their cost by 2025, facilitating widespread commercialization. SIBs are known for their safety under both low- and high-temperature conditions [8–11].

SIBs have emerged as a significant alternative to LIBs in meeting the escalating demands for large-scale energy storage applications. However, their overall performance currently falls short of that of LIBs. The primary challenge facing SIBs is their limited cycle life, primarily attributed to the large ionic radius and high mass of Na^+ ions, which hinder their transport and induce significant volume collapse and stress within the structure during intercalation/de-intercalation processes [12]. This structural degradation of the cathode materials leads to a shortened cycle life. Consequently, the development of highly stable electrode materials with robust frameworks is imperative to enable the reversible intercalation and de-intercalation of Na^+ ions. In SIBs, the existing anode materials generally exhibit a higher capacity than the cathodes. Therefore, the electrochemical characteristics, including the extent of the charge transfer and redox potential of cathode materials, largely determine the performance of SIBs. Moreover, the nature of the cathodes is identified as a major differentiating factor between LIBs and SIBs in terms of cost. The cost of producing cathodes from raw materials for both types of batteries is reported to be nearly identical. However, the cost reduction in SIBs primarily stems from the use of low-cost raw materials, leading to projected cost savings of 10–20% compared to LIBs. Specifically, the adoption of green and cobalt-free cathode materials renders SIBs sustainable, affordable alternatives to LIBs for large-scale energy storage and electric vehicle applications. Therefore, the development of suitable cathode materials is essential to enhancing the performance of SIBs [5,9,10,13].

A variety of cathode materials have been developed for use in SIBs. Some of the cathodes employed in SIBs include sodium pyrophosphate ($\text{NaMP}_2\text{O}_7/\text{Na}_2\text{MP}_2\text{O}_7$, where M = Ti, V, and Fe), layered transition metal oxides (AxTMO_{2+y} , where x is ≤ 1 , A = alkali metal, and TM (1 or 2) = Ti, V, Cr, Mn, Fe, Co, and Ni), perovskite transition metal fluorides (MF_3 and NaMF_3 , where M = Ni, Fe, and Mn), Prussian blue or hexacyanoferrates ($\text{KFeFe}(\text{CN})_6$) and organic polymers [14–17]. Among these options, vanadium-incorporated cathodes, which are naturally abundant and low cost, possess high theoretical capacities, energy densities, and operating voltages. Similar to sodium, vanadium is also abundant in the Earth's upper continental crust. The valence band electrons in vanadium ($3d^3 4s^2$) create a multivalent state (V^{2+} to V^{5+}), enabling rich electrochemical reactions compared to monovalent Na^+ ($3s^1$). Vanadium oxide (V_2O_5 and VO_2), sodium vanadium phosphates (NVPs, $\text{Na}_3\text{V}_2(\text{PO}_4)_3$, and NaVOPO_4), and sodium vanadium fluorophosphates (NaVPO_4F , $\text{Na}_3\text{V}_2(\text{PO}_4)_2\text{F}_3$) are typical vanadium-based cathodes utilized in SIBs. In assessing the suitability of cathode materials for SIBs, it is essential to compare the properties of key materials such as NVPs, NVPFs, and V_2O_5 . NVPs and NVPFs offer high theoretical capacities, typically around 117.6 mA h/g, with flat potential plateaus at approximately 3.4 V, ensuring stable voltage during cycling. The three-dimensional open framework of NVPs provides ample interfaces, ensuring high ionic mobility. However, both materials suffer from a limited cycle life due to the structural degradation caused by the large size of Na^+ ions, resulting in volume collapse and stress within the cathode structure. On the other hand, V_2O_5 exhibits moderate to high theoretical capacities and a generally better cycle life compared to NVPs and NVPFs. Additionally, V_2O_5 typically demonstrates better electronic and electrical conductivities, contributing to improved performance. While NVPs and NVPFs are derived from abundant and low-cost precursor materials, V_2O_5 may incur

higher processing costs. However, vanadium, the precursor of V_2O_5 , is relatively abundant in the Earth's crust. Overall, the choice of cathode material for SIBs depends on specific requirements such as the capacity, cycle life, cost, and environmental considerations [18].

Traditional synthesis methods typically yield microparticles for cathode materials. However, new material synthesis strategies have been explored to enhance the performance of these cathodes. Some of these strategies include the synthesis of nanomaterials, the creation of composites with conducting carbon materials and quantum dots, carbon composites, ion implantation, substitution of vanadium ions with Co^{2+} , and the preparation of porous materials using metal–organic framework (MOF) templates. Cathode materials with an interconnected hierarchical structure and surface modification have been found to be highly preferred and advantageous. Morphologies characterized by organized and interconnected pores of various diameters are termed hierarchically porous materials (HPMs) [19,20]. Nutshells, straws, and porous exoskeletons are among the naturally occurring HPMs. HPMs can be designed with dual (micro-mesoporous) and multiple porosities (macro-micro-mesoporous). The presence of pores in HPMs enhances the accessibility of reactants and leads to higher performance in applications where efficiency is correlated with the specific surface area. HPMs with higher surface areas, pore volumes, mass transfers, and storage capacities are preferred for SIBs. Typically, HPMs exhibit unique features such as micro- or sub-micro architectures with nanosized units, which facilitate ion diffusion and prevent internal stress. Synthesis methodologies that offer good control over the design, porous structure, size, geometry, and connectivity can yield efficient HPMs. Some advantages of HPMs include the (i) reduced agglomeration and contact resistance at interfaces, (ii) increased active sites, (iii) shorter ionic diffusion pathways, and (iv) enhanced electrolyte diffusion [21–24]. Their dual and multiple porosities significantly enhance ion diffusion and prevent internal stress, thus improving battery performance. Hence, it is crucial to highlight and account for the recent advancements in hierarchical porous structured cathodes, particularly those based on NVPs, NVFPs, and V_2O_5 . Accordingly, this review discusses the recent endeavors aimed at fabricating hierarchically porous NVP, NVPF, and V_2O_5 cathodes, as well as their performance characteristics.

2. Hierarchically Porous Cathodes Materials

Hierarchically engineered porous structured materials have received enormous attention in recent times, specifically due to the key significance of features like the high degree of assembly and ease of adaptation toward constantly evolving environmental conditions [25,26]. Most of the majestic living organisms on Earth are biologically composed of complex architectures enabling ‘aesthetics-to-uniqueness’ in their properties and functionalities. Multimodal porosity with space- or channel-engineered architectures with different length scales (micro (<2 nm), meso (2–50 nm), and macro (>50 nm)) are critical for the design, synthesis, and application of several structurally organized materials finding their expandability in advanced arenas from nanoscience to catalysis, energy conversion and storage, and several other industrially robust technologies [27].

Based on the unique properties of diverse materials, as shown in Figure 1, hierarchically pore-engineered structures are specifically assembled from ordered molecular units or as aggregates that are usually found in an intertwined/embedded fashion originating from atomic/nano/micro level variabilities, enhancing the diffusion kinetics with respect to the functional mechanisms of active electrodes (intercalation, (de)alloying, etc.) [28,29].

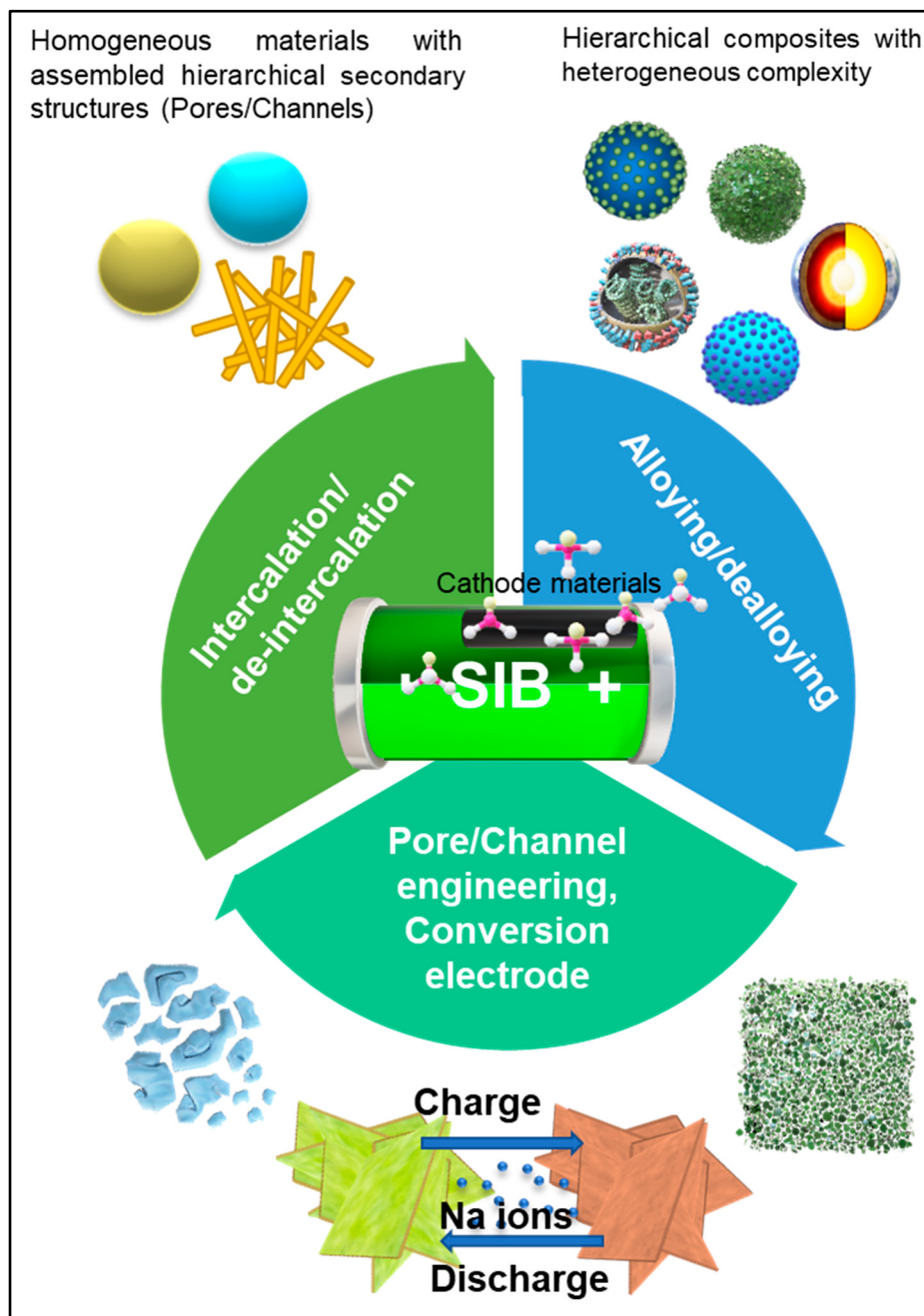


Figure 1. Salient features of hierarchically porous cathode material, where pore structures are usually found in an intertwined/embedded fashion. Atomic/nano/micro level structural features in hierarchically porous morphology improves the diffusion kinetics.

Depending on the combinations of synthetic strategies utilized for developing hierarchical porous materials, precise controllability from atomic-level regulation to nano/micro/macro architectures is designed to prevent nanoparticle agglomeration, longer diffusion lengths, and interfacial contact resistance [29]. Performance enhancement in SIBs has often been associated with the effective improvement of the electrochemical properties of cathode materials via hierarchical engineering of porous 3D or 2D framework structures with flexible alterations like surface treatment, appropriate doping at target lattices (doping with N, S, and Co), composites interconnected with heterogeneous carbon matrixes, and secondary structures formed from the assembly of homogeneous materials [20,29]. To be more precise, to improve the intrinsic electronic conductivity, specific rate capacity,

and long-cycle performance of SIBs, hierarchical pore-engineered structures such as vanadium pentoxide (V_2O_5), sodium vanadium phosphate ($Na_3V_2(PO_4)_3$, (NVP)), and sodium vanadium fluorophosphate ($Na_3V_2(PO_4)_3F$, NVPF) are the prominently studied cathode materials for SIBs in the recent times. In addition, some heterogeneous interconnections of these materials with conductive carbon composites are also widely explored. Henceforth, in this review, we spotlight the recent developments in the research methodologies adopted for hierarchical pore-engineering of active cathode materials.

3. Hierarchically Porous NVP Cathodes

NVP has emerged as one of the most promising cathode materials for SIBs due to its superionic conductivity, facilitated by a highly covalent open 3D framework, large interstitial spaces, high theoretical capacity ($117.6 \text{ mA h g}^{-1}$), and stable potential plateaus (around 3.4 V). NVP exhibits rapid charge/discharge rates, prolonged cyclic stability, and high energy density [30]. However, the larger particle size of NVP increases the diffusion pathway for Na^+ ions and electrons, which can hinder conductivity [31]. Additionally, the stress induced by large particles may compromise its structural integrity [32]. To address these challenges, various strategies have been employed to enhance the performance of NVP. Hierarchical porous structures of NVP have been developed to shorten the Na^+ diffusion pathway and improve the conductivity. These structures are fabricated using techniques such as sol-gel, hydrothermal, solvothermal, solution blending, spraying, solid-state annealing, electrospinning, and ball milling. Furthermore, methods like deposition of graphitized carbon (sp^2), ionic bulk doping, and formation of single crystal porous structures have been explored to optimize NVP's electrochemical properties.

3.1. NVP Cathodes by Sol-Gel Method

The sol-gel method is a simple, economical, and well-established approach suitable for large-scale preparation of nanomaterials with 3D porous structures [21]. During sol-gel synthesis, the precursors are uniformly mixed at the atomic or molecular level and allowed to undergo hydrolysis, leading to the formation of a 3D network through gelation and subsequent calcination steps. This method enables effective control over the stoichiometry and morphology by combining raw ingredients [33,34]. Electrospinning is another highly effective solution-processing method used for the fabrication of single- and multicomponent nanofibers and nanowires [35]. As the name implies, electrospinning involves the use of polymers or metal oxide sol-gels, where polymerized small molecules form an interconnected network. For the preparation of nanofibers via electrospinning, precise control of the stirring, viscosity, and aqueous content is crucial to achieve a solution that is suitable for spinning [36,37]. This method has been widely employed in the preparation of carbon-coated NVP hierarchical porous cathode materials (HPCMs). The cathode materials prepared using the sol-gel method, along with their preparation conditions and electrochemical performance, are provided in Table 1.

Table 1. Cathode material preparation conditions and electrochemical performance using the sol-gel method.

S. No.	Cathode Material	Method and Conditions	Modification	Specific Capacity (mA h/g—Current Rate (C))	% Stability/Number of Cycles—Current Rate (C)	Reference
1	$Na_3V_2(PO_4)_3$	Sol-gel—Sintering ($750\text{ }^\circ\text{C}/8\text{ h/Ar}$)	Carbon coating	91—80 C	64/10,000—100 C	[38]
2	$Na_3V_2(PO_4)_3$	Electrospinning of sol-gel—Sintering ($800\text{ }^\circ\text{C}/8\text{ h/Ar}$)	Carbon coating	116—0.1 C	88.6/150—0.5 C	[39]

Table 1. Cont.

S. No.	Cathode Material	Method and Conditions	Modification	Specific Capacity (mA h/g—Current Rate (C))	% Stability/Number of Cycles—Current Rate (C)	Reference
3	Na ₃ V ₂ (PO ₄) ₃	Sol-gel—Sintering (800 °C/8 h/N ₂)	NVP grown in porous carbon network	116.2—0.2 C	82.1/10,000—20 C	[40]
4	Na ₃ V ₂ (PO ₄) ₃	Sol-gel—Sintering (450 °C/4 h; 700 °C/6 h/N ₂)	Doping K/Co and integrating carbon quantum dots	109.8—5 C	87.6/400—5 C	[41]
5	Na ₃ V ₂ (PO ₄) ₃	Sol-gel—Sintering (350 °C/5 h; 800 °C/8 h/N ₂)	Carbon composite	119.5—0.1 C	90.2/500—10 C	[42]

To overcome the challenges associated with insufficient carbon coating and the polarization of milled micron-sized NVP HPMs, Rui et al. devised a novel approach involving the development of a meso- and macroporous hybrid nanocomposite of NVP/reduced graphene oxide (rGO). In their methodology, a combination of freeze-drying and post-calcination techniques was employed. Initially, NVP precursors, rGO, and poly(vinylpyrrolidone) (PVP) were mixed in solution, followed by freeze-drying, as schematically depicted in Figure 2b. This freeze-drying-assisted method enabled the formation of a three-dimensional hierarchical structure composed of meso- and macroporous NVP@C@rGO cathode material, facilitating pathways for electron and sodium ion transport, as illustrated in Figure 2a. During the subsequent heat treatment at 750 °C for 8 h under Ar/H₂ conditions, PVP functioned as a chelating agent, while RGO served as a conducting carbon source. Moreover, PVP contributed to the formation of a nanoporous carbon matrix, providing a scaffold for the growth of crystalline NVP nanoparticles. The nanoporous carbon matrix and RGO nanosheets confined the space during calcination, thereby restricting further growth of the NVP nanoparticles. The resulting NVP/RGO cathode exhibited promising electrochemical performance, as evidenced by the electrochemical impedance spectra shown in Figure 2c, obtained at the third fully discharged state. Moreover, the energy density versus power density performance of the NVP@C@rGO cathode material was evaluated and compared with several advanced lithium-ion battery and sodium-ion battery cathodes, as illustrated in the Ragone plots in Figure 2d. The long-term cycling stability of the NVP@C@rGO cathode material was also demonstrated over 10,000 cycles at a rate of 100 C, as depicted in Figure 2e. The good performance of the NVP/RGO hybrid cathode can be attributed to its ultrafast charge and discharge rates, short Na-ion diffusion length, and the macro/mesoporous morphology capable of buffering the strain-induced volume changes during the charge/discharge processes [38].

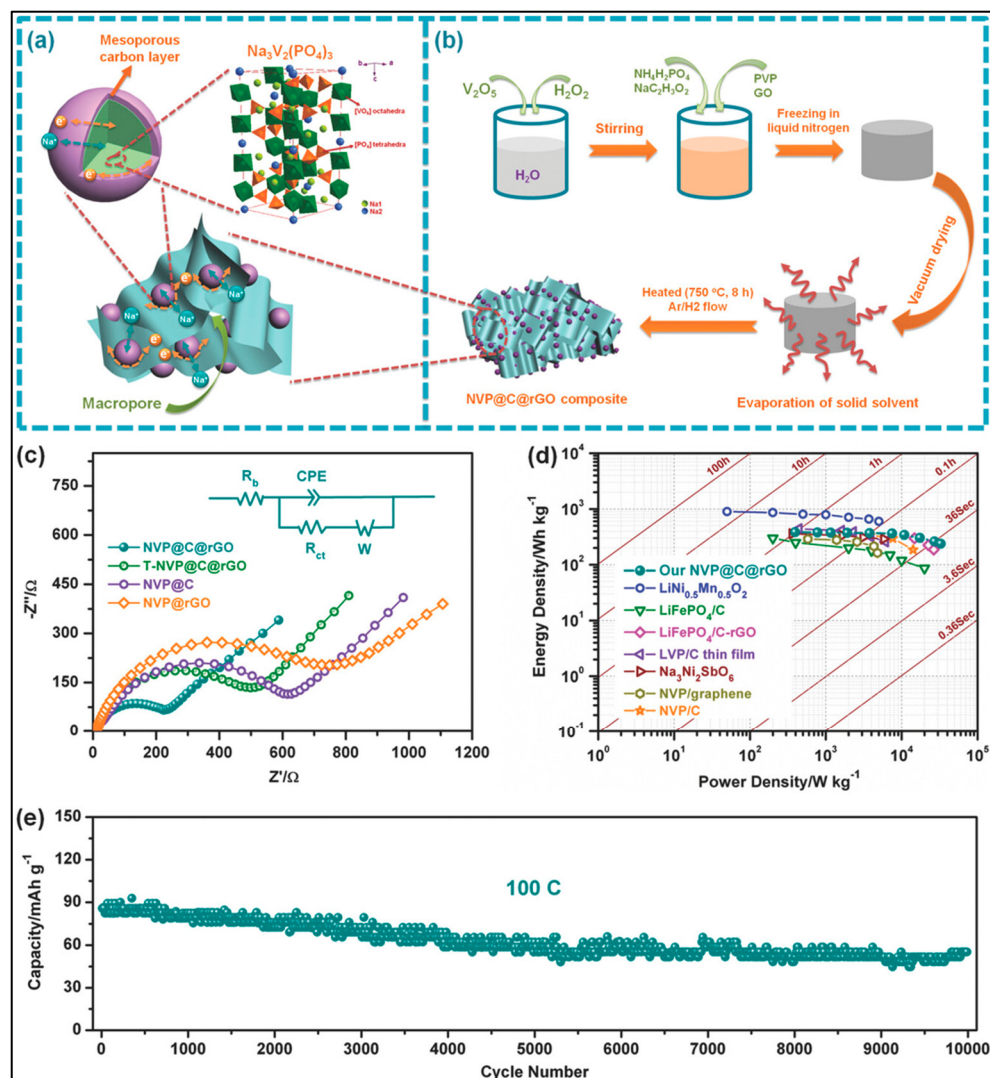


Figure 2. (a) Illustration depicting a three-dimensional hierarchical structure composed of meso- and macroporous NVP@C@rGO cathode material, featuring pathways facilitating electron and sodium-ion transport. In the upper-right corner, a crystal structure diagram of the NA-SICON-type $\text{Na}_3\text{V}_2(\text{PO}_4)_3$ is provided for reference. (b) Schematic representation of the freeze-drying-assisted method utilized in the synthesis of the NVP@C@rGO composite material. (c) Electrochemical impedance spectra obtained at the third fully discharged state, along with the corresponding fitted equivalent circuit model (inset). Key parameters include the R_b (bulk resistance), R_{ct} (charge transfer resistance), CPE (constant phase element), and W (Warburg impedance). (d) Ragone plots illustrating the energy density versus power density performance of the NVP@C@rGO cathode material compared with several advanced lithium-ion battery (LIB) and sodium-ion battery (NIB) cathodes. (e) Long-term cycling stability of the NVP@C@rGO cathode material demonstrated over 10,000 cycles at a rate of 100 C [38].

Ni et al. explored the utilization of the electrospinning technique to fabricate flexible three-dimensional electronic channels comprising interconnected carbon nanofibers (CNFs) enveloped with NVP particles, as illustrated in the procedural steps depicted in Figure 3a'. The NVP precursor was synthesized via the sol-gel method, involving the stirring of a mixture containing stoichiometric amounts of NH_4VO_3 , $\text{NH}_4\text{H}_2\text{PO}_4$, citric acid, and NaOH at 80°C until a blue sol-gel formed. Following drying and annealing in a muffle furnace at 350°C for 3 h, the NVP precursor was obtained. In the subsequent phase, a composite solution comprising 1 g of poly(acrylonitrile) (PAN, Mw = 150,000) and 8.3% NVP (based on the weight of the polymer matrix) dissolved in 12 mL of DMF was electrospun using

a 21 G nozzle under a voltage of 18 kV. The resultant NVP-containing polymer web was then heat-stabilized in air at 280 °C for 2 h and carbonized in an argon atmosphere at 800 °C for 8 h, yielding free-standing CNFs embedded with NVP. This configuration enhanced the electrolyte wettability, thereby facilitating full Na⁺ extraction and insertion, as demonstrated in the electrochemical assessments of the NVP-freestanding//liquid electrolyte//NaTi₂(PO₄)₃@C full battery shown in Figure 3e. Furthermore, the CNFs, besides providing conducting pathways, played a crucial role in preventing the agglomeration of the NVP particles. The resulting electrode exhibited a reversible specific capacity of 116 mA h/g at 0.1 C, corresponding to 99% of the theoretical specific capacity, with 88.6% of the initial capacity retained after 150 cycles at 5 C. These promising results indicate the potential of these cathodes for applications in wearable and flexible energy storage devices based on SIBs, offering advantages such as reduced overall weight and enhanced volumetric energy and power density compared to traditional pasted plate electrodes [39].

To simplify and reduce the costs of the production of NVP/C, Zhu et al. developed a sol-gel method. They utilized a hierachal porous carbon matrix (with a surface area of 2463 m²/g and a pore volume of 2.362 cm³/g) prepared from gelatin through spray pyrolysis, while the NVP precursors were converted into a gel. This gel was then dried and sintered at 800 °C for 8 h under N₂ conditions, resulting in a hierachal carbon framework embedded with NVP nanoparticles. During this process, the NVP precursors were absorbed into the carbon matrix, facilitating the confined growth of NVP nanoparticles. The cathode exhibited a specific capacity of 116.2 mAh/g at 0.2 C, with a capacity retention of 82.1% after 10,000 cycles (measured at 20 C). The unfilled pores in the carbon matrix facilitated ion transport and contributed to capacity improvement. This sol-gel-derived pore-confined NVP/C cathode material shows promise for the production of low-cost SIBs [30].

Tian et al. employed a strategy involving the bulk doping and integration of carbon quantum dots (CQDs) with NVP. By combining semiconducting CQDs with the mixed ionic conductor NVP, they established a heterojunction structure that enhanced the electronic mobility. Additionally, the bulk doping of NVP with K/Co was anticipated to bring about a synergistic effect, as K and Co occupy Na1 and V sites in the NVP crystal, respectively. It is well-known that CQDs serve as electron carriers, while K and Co act as hole carriers. The precursors of CQDs, NVP, K, and Co were solution mixed, freeze-dried, and subjected to a two-step calcination process (450 °C for 4 h, and 700 °C for 6 h) under N₂ conditions. This resulted in the generation of a composite NVP cathode with a p(K/Co)-n(CQD)-type interfacial heterojunction. The cathode exhibited a reversible capacity of 109.8 mAh/g at 5 C and maintained 87.6% stability after 400 cycles (at 5 C). The synergistic heterojunction enhanced the electron mobility by reducing the scattering and collision caused by anion dopants [41].

Wang et al. devised a surfactant-assisted molding method for preparing NVP/C HPMs, utilizing the sol-gel synthesis technique. Cetyltrimethylammonium bromide (CTAB) was employed as a surfactant to facilitate micelle formation. By adjusting the solvent concentration, the morphology of the micelles could be varied from plate-like to spherical and chain-like structures. The gel formed from the NVP precursors and surfactant was blast-dried at 350 °C for 5 h under N₂ and then calcined at 800 °C for 8 h under N₂. Through optimization of the synthesis conditions, 3D interconnected NVP HPMs were obtained. When subjected to cyclic stability testing (500 cycles at 10 C), the cathode retained 90.2% of its initial reversible capacity (61.3 mA h/g at 10 C). The authors emphasized that alterations in the solvent composition resulted in NVP with different pore structures. Specifically, by adjusting the volume ratio of ethanol to water, NVP with varying pore structures, interconnectivity, and surface areas could be controlled. A volume ratio of 4:6 ethanol to water yielded NVP/C HPMs with excellent electrochemical properties, suggesting that this method could be adopted for cost-effective industrial production of NVP/C cathodes [42].

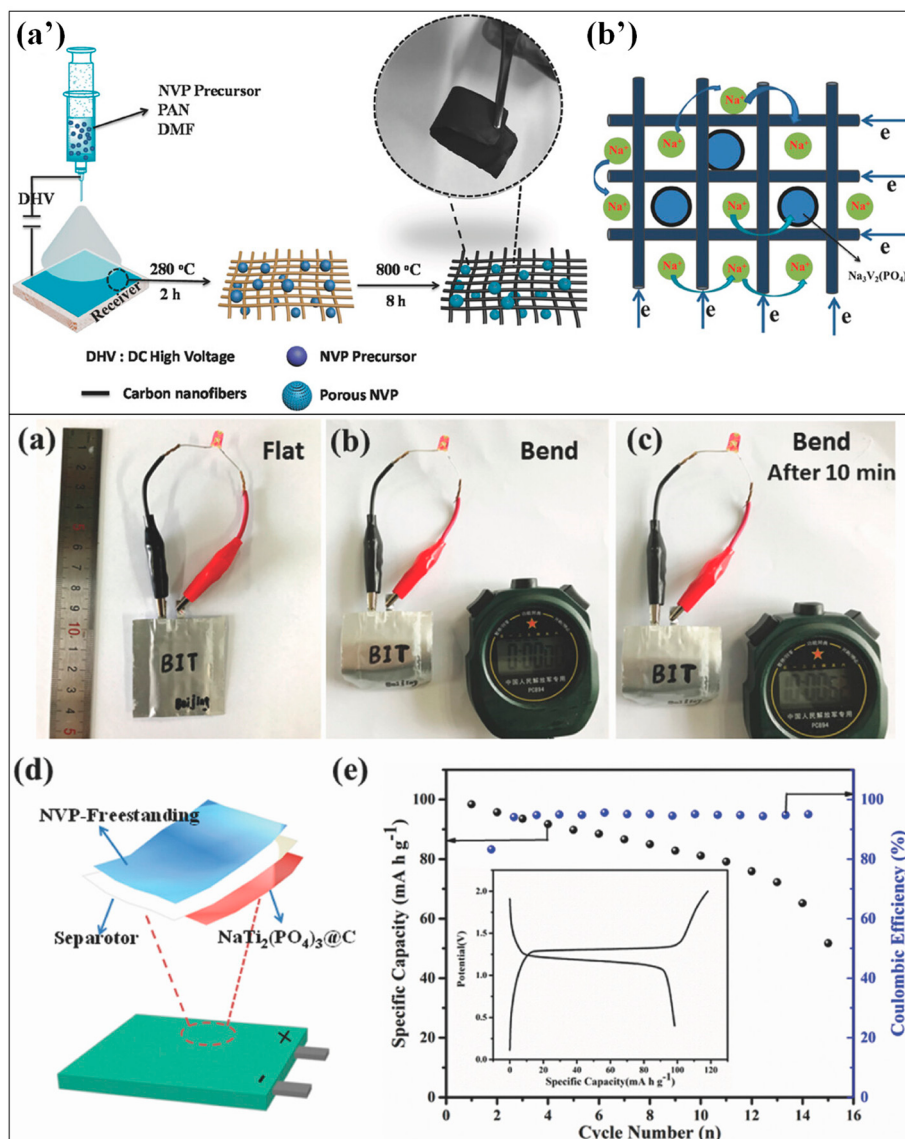


Figure 3. (a') Diagram illustrating the procedural steps involved in preparing the NVP-freestanding composite material. (b') Depiction of the electronic and Na⁺ diffusion pathways within the three-dimensional structure. Digital images showcasing the sodium-ion soft package battery: (a) in a flat state, (b) in a bent state, (c) in a bent state after 10 min, and (d) revealing the internal structure of the flexible sodium-ion soft package battery. (e) Electrochemical assessments of the NVP-freestanding//liquid electrolyte//NaTi₂(PO₄)₃@C full battery: cycling performance at a current density of 20 mA g⁻¹, and the initial charge–discharge curve within a potential window of 0.4–2 V (inset) [39].

3.2. NVP Cathodes by Hydrothermal Method

Hydrothermal synthesis is a versatile and unique method capable of crystallizing materials in an aqueous medium under high-temperature and -pressure conditions [43]. In this typical synthesis process, the precursors are loaded in the form of a solution, slurry, or gel and subjected to high pressure and temperature using Teflon-lined autoclaves [44,45]. To further enhance the crystallinity and remove organic templates or residues, post-hydrothermal sintering is often necessary [46]. The advantages of the hydrothermal method over other traditional synthesis routes include (i) the ability to produce quasi-phase materials; (ii) the lower reaction temperatures compared to solid-state synthesis; (iii) the high reaction rates; (iv) the greater control over crystal growth and morphology; and (v) the production of crystalline materials with homogeneous dispersion. This method facilitates

the preparation of NVP HPMs with the desired nanostructures and short diffusion lengths. Hydrothermal synthesis is particularly suitable for achieving NVP HPMs with a high surface area, structural confinement, and carbon coating [47]. It is noteworthy that, compared to the solvothermal method, the hydrothermal method is predominantly used for the preparation of NVP HPMs. The cathode materials prepared using the hydrothermal method, along with their preparation conditions and electrochemical performance, are provided in Table 2.

Table 2. Cathode material preparation conditions and electrochemical performance using the hydrothermal method.

S. No.	Cathode Material	Method and Conditions	Modification	Specific Capacity (mA h/g—Current Rate (C))	% Stability/Number of Cycles—Current Rate (C)	Reference
1	Na ₃ V ₂ (PO ₄) ₃	Hydrothermal (200 °C/12 h)—Sintering (350 °C/3 h/Ar; 750 °C/8 h/Ar)	Carbon coating	102.1—1 C	74.4/600—1 C	[48]
2	Na ₃ V ₂ (PO ₄) ₃	Hydrothermal (180 °C/24 h)—Sintering (350 °C/4 h/Ar; 750 °C/6 h/Ar)	Carbon coating	114.8—1 C	81.27/8000—20 C	[49]
3	Na ₃ V ₂ (PO ₄) ₃	Hydrothermal (200 °C/48 h)—Sintering (350 °C/4 h/Ar; 750 °C/6 h/Ar)	Carbon coating	99.3—100 C	79.1/1000—20 C	[50]
4	Na ₃ V ₂ (PO ₄) ₃	MOF by hydrothermal (180 °C/12 h; 450 °C/4 h)—Solution blending with NVP precursors—Sintering (800 °C/8 h)	Carbon composite	111.2—1 C	97.8/500—1 C	[51]

The durability of high-surface-area NVP/C materials grown without space confinement is often compromised due to their tendency to agglomerate easily. In pursuit of long-term stability, Li et al. devised a method to prepare carbon-coated NVP nanowalls via the hydrothermal approach (200 °C for 12 h). In this process, the NVP precursors were combined with hydrazine hydrate (a reducing agent), 1,4-dihydroxy-2-butyne (a carbon source), and NaOH (an additive compensating for the loss of Na). The solid products obtained from the hydrothermal step were preheated (350 °C for 3 h under Ar) and sintered (750 °C for 8 h under Ar) to produce NVP/C nanowalls. This cathode demonstrated a remarkable 74.4% capacity retention after 600 cycles, with an initial specific capacity ranging from 99.1 to 107.9 mAh/g at 1 C. At various current densities (0.1, 0.2, 0.5, 1, and 2 C), specific capacities of 107.9, 106.4, 104.5, and 102.1 mAh/g were observed, respectively. This performance surpassed that of irregularly shaped NVP/C materials. The superior electrochemical performance of NVP/C nanowalls was attributed to their short ion diffusion pathways and high specific surface area [48].

With the aim of simplifying the structure and overcoming the synthesis complications, Ling et al. prepared NVP/C using the hydrothermal method. In this process, an aqueous solution containing NVP precursors, surfactants, and carbon sources (PEG-4000 and sodium dodecyl benzene sulphonate) was hydrothermally treated at 180 °C for 24 h. The resulting suspended mass was recovered, dried, milled, and heat-treated under Ar atmospheres (350 °C for 4 h and 750 °C for 6 h). The resulting NVP/C material exhibited a hierarchical porous structure, with carbon layers deposited *in situ* on the generated NVP

nanosheets. The interlinking of NVP nanosheets led to the formation of a hierarchical porous structure containing meso-, micro-, and macropores. The carbon capping layer on the NVP nanosheets assembled into a conductive matrix, limiting the grain size by restricting growth. The NVP/C cathodes demonstrated a specific capacity of 114.8 mAh/g at 1 C, close to the theoretical value, and maintained 81.27% stability after 8000 cycles (at 20 C), with a rate capacity of 89.3 mAh/g at 60 C. Importantly, this method was suggested as a useful strategy for the large-scale synthesis of high-performance NVP/C cathodes [49].

The hydrothermal method is also employed for the preparation of hierarchically porous NVP/C microspheres, where NVP nanoflakes are interconnected and assembled. In this process, the NVP precursors and sodium oleate (acting as both surfactant and carbon source) undergo reflux (80 °C for 10 h) followed by hydrothermal treatment (200 °C for 48 h). The hydrothermal process results in a self-assembled cylindrical hydrogel, which is then freeze-dried and annealed (800 °C for 8 h) to yield NVP/C hierarchically porous microspheres. The carbon layers are doped with nitrogen. The NVP/C microspheres exhibit a rate capability of 99.3 mA h/g at 100 C and retain 79.1% of the initial capacity (105.9 mA h/g at 100 C) after 10,000 cycles (at 20 C). When incorporated into a SIB with a full-cell configuration, this cathode achieves a practical energy density of 223 Wh/kg. The hierarchical porous structure and N-doped carbon layer capping facilitate a bi-continuous pathway for electron/ion transfer and ensure robust structural integrity. This method is found to be suitable for obtaining NVP/C microsphere cathodes with promising electrochemical performance [50].

Chen et al. utilized a metal–organic framework (MOF) precursor to obtain NVP/C HPMs. The central metal ion and organic ligands in the MOF structure served as a template for preparing micro-nano structured NVP/C HPMs. MOFs offer the advantage of in situ generation of particles of metals, metal oxides, phosphates, phosphides, and sulfides. Upon the burning of organic ligands, they produce a large quantity of gas and leave behind HPMs with a uniform in situ carbon coating on NVP particles. Unlike pure nanomaterials with high surface energy, MOF-derived HPMs are expected to have minimal agglomeration. Chen et al. initially obtained a vanadium oxide/C composite by calcining an MOF hydrothermally prepared using VCl₃ and 1,4-naphthalenedicarboxylic acid. Subsequently, the vanadium oxide/C was blended with an aqueous solution of NaH₂PO₄ and citric acid mixture, along with ethanol. The resulting powder obtained upon evaporation of this mixture was then calcined at 800 °C to obtain the MOF-based NVP/C (M-NVP/C) composite. The M-NVP/C composite demonstrated a specific capacity of 111.2 mAh/g at 1 C, with 97.8% capacity retention over 500 cycles at 1 C. This performance surpassed that of sol-gel synthesized NVP/C (82.6 mAh/g and 85.5% stability over 1000 cycles at 5 C). The improved performance of M-NVP/C was attributed to its hierarchically porous structure with a highly conductive 3D network connecting the surface and particles [51].

3.3. NVP Cathodes by Solution Blending and Spraying Methods

Solution blending represents a direct and straightforward approach, wherein functional components are mixed in a solvent medium, allowing them to blend together or react to form a composite precursor. The precursor derived from solution blending is then dried and sintered to yield crystalline functional materials [52,53]. Mechanical-stirring, reflux, shear-mixing, and sonication procedures are often employed to aid the blending process [54]. In solution spraying, the spray formulation prepared using solution-blended precursors is sprayed into the desired droplets, which are then dried and sintered. To facilitate the transition from liquid to solid, easily volatile and low-boiling organic solvents are commonly used in the spraying formulation. Alongside water, low-boiling solvents such as tetrahydrofuran and ethanol are often utilized. The solution method enables the dispersion of previously synthesized nanomaterials within the host material matrix. To assemble into porous structures, surfactants capable of forming self-assemblies such as micelles are employed as soft templates. In some cases, these organic templates also serve as precursors for carbon coating on NVP HPMs. The cathode materials prepared using

the solution blending and spraying methods, along with their preparation conditions and electrochemical performance, are provided in Table 3.

Table 3. Cathode material preparation conditions and electrochemical performance using the solution blending and spraying methods.

S. No.	Cathode Material	Method and Conditions	Modification	Specific Capacity (mA h/g—Current Rate (C))	% Stability/Number of Cycles—Current Rate (C)	Reference
1	Na ₃ V ₂ (PO ₄) ₃	Coprecipitation—Sintering (650 °C/6 h/Ar-H ₂ (95:5))	Carbon coating	62—40 C	50/30,000—40 C	[55]
2	Na ₃ V ₂ (PO ₄) ₃	Solution blending—Sintering (700 °C/6 h/Ar-H ₂ (95:5))	Carbon coating	102.31—1 C	90.9/10,000—1 C	[56]
3	Na ₃ V ₂ (PO ₄) ₃	Solution blending (350 °C/20 min/Air; 850 °C/6 h/Ar)	Carbon composite	113—1 C	88.1/200—1 C	[57]
4	Na ₃ V ₂ (PO ₄) ₃	Pyrolysis (350 °C/5 h/N ₂ ; 700 °C/8 h/N ₂)	Carbon coating	131—20 C	61.83/10,000—20 C	[58]

Saravanan et al. endeavored to realize the preparation of NVP/C cathodes using a low-temperature and less time-consuming method. They employed the soft template method, wherein a cationic surfactant (CTAB) and NVP were mixed in solution, dried by evaporation, and annealed at 650 °C for 6 h under Ar-H₂ (95:5) conditions. The annealing process removed the organic template and facilitated the cross-linking of the inorganic matrix. The resulting NVP/C composites contained 6 wt.% carbon content. This material exhibited good Na⁺ storage, with a specific capacity of 62 mAh/g at 40 °C and 50% capacity retention after 30,000 cycles at 40 °C. The authors predicted that these findings hold potential for the development of SIB applications aimed at storing renewable energy sources [55].

Wei et al. proposed a synthesis strategy for preparing NVP/C by combining soft-chemistry solution mixing and post-calcination. The NVP precursor solution was mixed with chemically exfoliated graphene oxide (GO), and the solvent was evaporated to yield a powder, which was then calcined at 750 °C under an Ar:H₂ (95:5) atmosphere. This process resulted in the formation of NVP/C hollow nanospheres with a hierarchically porous structure. These nanospheres exhibited ultra-long stability, with 90.9% capacity retention after 10,000 cycles at 1 C. The initial reversible capacity was measured at 102.31 mA h/g at 1 C. The conducting carbon network and hierarchical pore structure in the hollow nanospheres ensured barrier-free diffusion of Na⁺ ions and ultrafast electron transfer [56].

Carbon-coated NVP HPMs have been favored for achieving cathodes with enhanced rate performance and an extended cycle life. The carbon coating serves to augment the electrical conductivity of NVPs. Salehi et al. devised a method to prepare carbon-coated NVP HPMs using a soft template approach, employing a mixture of CTAB and glycine. The resulting carbon-coated NVP HPMs (NVP/C) were obtained by drying the aqueous mixture at temperatures below 100 °C and calcining the resultant mass at temperatures exceeding 700 °C. During calcination, the organic molecules were incinerated, leaving behind a composite of platelet-shaped and spongy NVP/C with high porosity and surface area (6–7 m²/g). The pore volume and size of NVP/C ranged from 0.02 to 0.5 cm³/g and 1 to 30 nm, respectively, with a carbon layer thickness of approximately 6 nm. Optimal results were achieved using a combination of 0.4 mmol CTAB and 0.4 mmol glycine, yielding spongy NVP/C composed of platelet-shaped NVP particles. The graphitic nature

of the amorphous carbon coating on the NVP supported electronic conductivity. The NVP/C composite exhibited a high specific capacity of 113 mAh/g at 1 C, with 88.1% capacity retention after 200 cycles at 1 C and a rate performance of 96 mAh/g. The improved electrochemical performance was attributed to the unique spongy structure, which provided abundant active sites and accommodated volume expansion during the charge/discharge process [57].

NVP/C HPMs have predominantly been synthesized with nano- or micron-sized NVPs stacked into porous structures. However, single crystal porous NVP/C configurations offer the advantage of shorter Na^+ -ion diffusion pathways compared to stacked structures. Xiong et al. devised a versatile polymer template-based strategy for synthesizing single crystal porous NVP/C materials. In this method, NVP precursors were mixed with PVP in a spray formulation containing a solvent mixture of tetrahydrofuran, ethanol, and water. This formulation was then sprayed into droplets, which were subsequently aged and pyrolyzed at 350 °C for 5 h and 700 °C for 8 h in a N_2 atmosphere.

The proposed mechanism for the formation of hierarchically porous NVP single crystals using the polymer-stabilized droplet template approach is depicted in Figure 4a'. The size of the droplets was controlled to regulate the size of the NVP crystals. PVP served as a stabilizer and minimized the thermodynamically repulsive forces between the templates and NVP precursors. The single crystal NVP exhibited remarkable electrochemical performance, with a rate capability of 61 mAh/g at 100 C, stability of 61.83% over 10,000 cycles at 20 C, and reversible capacity of 131 mAh/g at 20 C. Figure 4 illustrates the electrochemical profiles and sodium-ion transport characteristics of Macro-NVP, SMeso-NVP, HP-NVP, and WMeso-NVP. The presence of interconnected pores in the single crystal structure was attributed to the observed electrochemical performance. These interconnected pores facilitated facile solid–liquid Na^+ transfer, increased the electrolyte/electrode contact area, and provided a shorter ion diffusion pathway [58].

3.4. NVP Cathodes by Solid State Synthesis

In solid-state synthesis, the precursors are either mixed in a solid state or transformed into solid powder after solution blending. To achieve a solid-state mixture, appropriate tools such as ball milling, manual or mechanical grinding are utilized [59]. Compared to manual mixing, solution blending followed by mechanical solid mixing offers a more homogeneous mixture. Maximum homogenization of the constituents is preferred to ensure uniformity [60]. The resulting powder mixture is then subjected to high-temperature sintering, with or without low-temperature pre-sintering. The advantages of solid-state synthesis include its simplicity, time efficiency, and cost-effectiveness [61]. Additionally, the minimal or non-usage of solvents reduces environmental pollution [62]. Furthermore, the absence of a liquid medium eliminates mixing issues related to the viscosity gradient and miscibility, allowing for the inclusion of a maximum number of solid constituents to cover various functionalities. Solid-state synthesis has been employed for the preparation of multi-atom doped and carbon-coated NVP HPMs. The cathode materials prepared using solid-state synthesis, along with their preparation conditions and electrochemical performance, are provided in Table 4.

To meet the requirements for high-power applications, large-sized NVP with high-rate capability is preferred. Fang et al. synthesized NVP/C using a pre-reduction and calcination route. Initially, NVP particles were prepared by mixing NVP precursors through high-energy ball milling (2 h/Ar atmosphere), followed by drying into powder (80 °C for 6 h) and sintering at 850 °C for 8 h under Ar:H₂ (95:5) conditions. Subsequently, the synthesized NVP particles were further heated in a furnace to 600 °C in an Ar atmosphere, after which Ar:acetylene gas was purged. The furnace was then heated to 690 °C and kept for 20 min, with acetylene serving as the carbon source. This process led to the formation of an NVP/hierarchical carbon cathode material. This cathode demonstrates a reversible capacity of 115 mA h/g at 0.2 C, close to the theoretical value. The rate capability was 38 mA h/g, and cyclic stability reached 54% after 20,000 cycles at 30 C. Between

the NVP particles, an interconnected carbon framework formed a conducting pathway akin to electronic wiring. The carbon matrix also functioned as a buffer, accommodating volume changes. Moreover, the hierarchical carbon proved beneficial for producing NVP/C cathodes capable of fast ion transport and good electrochemical performance [63].

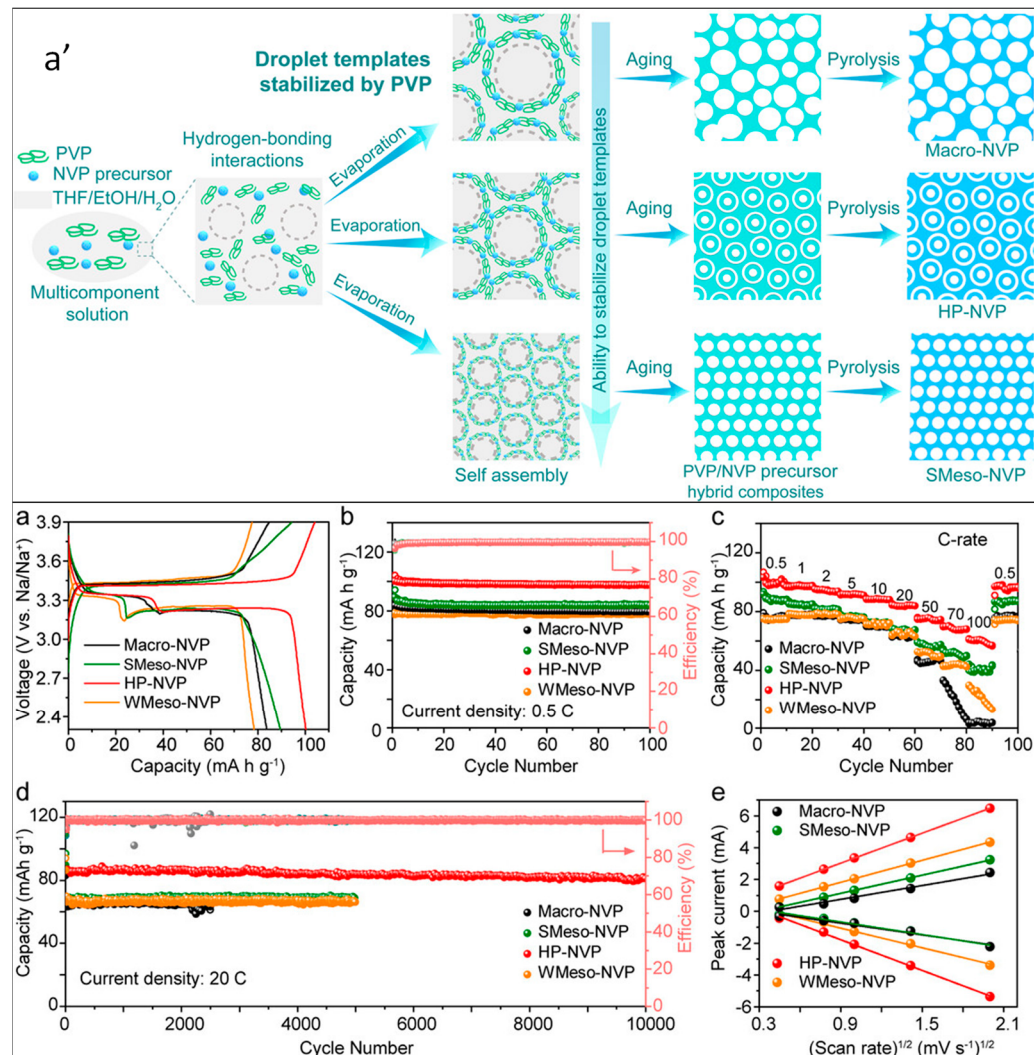


Figure 4. (a') Proposed mechanism for the formation of hierarchically porous NVP single crystals using the polymer-stabilized droplet template approach. Evaluation of the electrochemical performance and sodium-ion transport characteristics of Macro-NVP, SMeso-NVP, HP-NVP, and WMeso-NVP. (a) Initial charge–discharge profiles. (b) Cycling performance at a rate of 0.5 C. (c) Rate performances ranging from 0.5 to 100 C. (d) Long-term cycling stability at a rate of 20 C. (e) Linear regression analysis for the anodic and cathodic peak currents observed in CV curves at various scan rates [58].

Table 4. Cathode material preparation conditions and electrochemical performance using the solid-state synthesis.

S. No.	Cathode Material	Method and Conditions	Modification	Specific Capacity (mA h/g—Current Rate (C))	% Stability/Number of Cycles—Current Rate (C)	Reference
1	Na ₃ V ₂ (PO ₄) ₃	Ball milling—Sintering (800 °C/8 h/Ar/H ₂ (95:5))	Carbon coating	115—0.2 C	54/20,000—30 C	[63]
2	Na ₃ V ₂ (PO ₄) ₃	Mixing by ball milling—Sintering (350 °C/4 h/H ₂ /N ₂ ; 700 °C/12 h/H ₂ /N ₂ (8:92))	N/S doping and copper coating	113—1 C	82.1/5000—50 C	[64]
3	Na ₃ V ₂ (PO ₄) ₃	Forming slurry by stirring—Sintering (750 °C/8 h/Ar/H ₂)	Carbon composite	103.4—1 C	78.2/2000 at—10 C	[65]
4	Na ₃ V ₂ (PO ₄) ₃	Mixing by ball milling—Sintering (800 °C/8 h/Ar/H ₂ (95:5))	Carbon coating	114.2—0.5 C	52/10,000—20 C	[66]

NVP HPMs coated with multi-heteroatom-doped carbon material have proven useful for enhancing electrochemical properties. Liang et al. modified NVP by depositing a sulfur- and nitrogen-doped carbon coating. The NVP precursors were mixed with sulfur (and benzyl disulfide) and nitrogen (urea) sources by milling, then subjected to a two-step sintering process (350 °C for 4 h; 700 °C for 12 h) under an H₂:N₂ (8:9) atmosphere. The multiatom-doped carbon network on the NVP decreased the internal resistance and prevented NVP agglomeration. This material delivered a discharge capacity of 113.0 mAh/g at 0.2 C, with 82.1% stability after 5000 cycles at 30 C. The well-interconnected carbon layer effectively enhanced electron and ion transport. Defect sites created by nitrogen and sulfur doping shortened the ion diffusion pathways, resulting in high capacity retention. This approach is suitable for preparing various multiatom-doped cathodes and provides insights for large-scale production [64].

Li et al. developed a surfactant-assisted solid-state annealing method for preparing nanoflake-assembled hierarchically porous NVP/C microflowers, using sodium oleate as both a sodium and carbon source. Initially, vanadium pentoxide, hydrogen peroxide, sodium oleate, and ammonium dihydrogen phosphate (in a 2:3:3 molar ratio of V:P:Na) were stirred at 70 °C to form a viscous slurry, which was then annealed at 750 °C for 8 h under an Ar:H₂ atmosphere. The resultant NVP/C HPMs exhibited a self-assembled nanoflake structure, with the microflowers composed of several self-assembled flakes, each with a thickness of several tens of nanometers. Pores were distributed from the center to the exterior, with the porous area occupied by loosely interconnected flakes. By tuning the annealing temperature, the ordered and flaky structure could be varied, with 750 °C being optimum for preparing cathodes exhibiting high specific capacity (103.4 mAh/g), cyclic stability, and rate performance (68.3 mAh/g), along with good cycling stability (78.2% after 2000 cycles). The self-assembled flakes organized in the microflower structure provided an enlarged electrode–electrolyte interface, accommodating the volume changes that occurred during cycling and improving the structural integrity. The in situ generated carbon coating increased the conductivity and prevented the agglomeration of NVP/C. This method is simple and promising for large-scale production of NVP/C HPM-based cathodes for SIBs [65].

The solid-state reaction strategy was also employed for preparing NVP/C HPMs. Zhao et al. utilized a facile molten hydrocarbon-assisted method, where the surfactant Span 80 was used as a carbon source. The mixture of NH₄H₂PO₄, Span 80, paraffin,

$\text{VOC}_2\text{O}_4 \cdot 1.4\text{H}_2\text{O}$, and CH_3COONa was milled together and then heat-treated at 800°C under an Ar:H_2 atmosphere. Figure 5a' illustrates the proposed mechanism for the formation of $\text{Na}_3\text{V}_2(\text{PO}_4)_3$ nanoflakes. The resultant NVP/C material exhibited an interconnected hierarchical nanoarray structure with large open spaces. The heating rate played an important role in the formation of the hierarchical porous structure, which was composed of ultrathin NVP nanoflakes coated with a partially graphitized carbon layer that improved the conductivity and structural integrity. Figure 5a–e present the electrochemical characterization of the synthesized $\text{Na}_3\text{V}_2(\text{PO}_4)_3$ nanoflakes as a half-cell cathode within the potential range of $2.5\text{--}4.0\text{ V}$ versus Na/Na^+ . The optimized sample demonstrated a reversible capacity of 114.2 mAh/g at 0.5 C , with 76.8% stability after 10,000 cycles at 10 C (0.0048% capacity loss per cycle). The hierarchical porous array structure provided ample space for Na^+ -ion diffusion and reduced stress during the charge–discharge process [66].

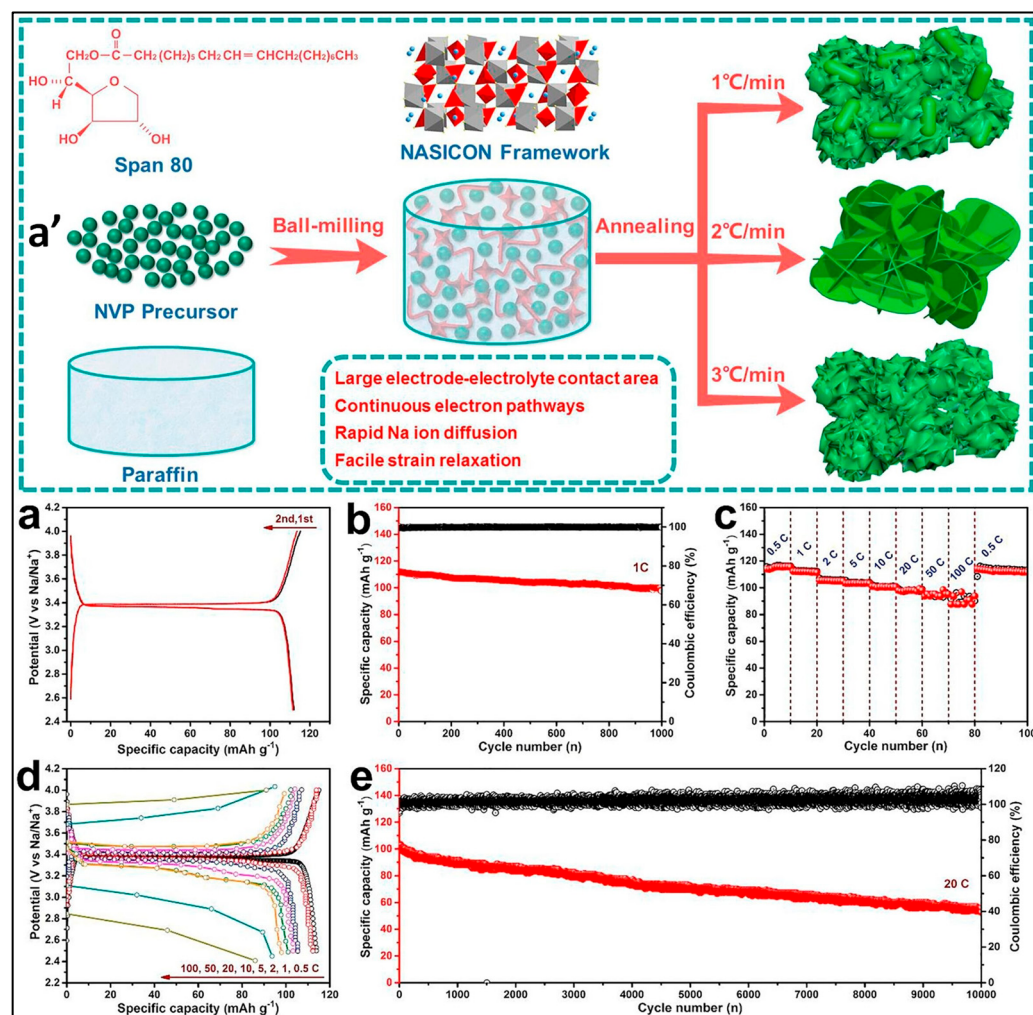


Figure 5. (a') Diagram illustrating the proposed mechanism for the formation of $\text{Na}_3\text{V}_2(\text{PO}_4)_3$ nanoflakes. Electrochemical characterization of the synthesized $\text{Na}_3\text{V}_2(\text{PO}_4)_3$ nanoflakes as a half-cell cathode within the potential range of $2.5\text{--}4.0\text{ V}$ versus Na/Na^+ . (a) First and second charge–discharge curves at a current density of 1 C . (b) Cycling performance at 1 C . (c) Rate performance. (d) Corresponding charge–discharge curves of the $\text{Na}_3\text{V}_2(\text{PO}_4)_3$ nanoflakes. (e) Demonstrated ultralong-life cycling performance and Coulombic efficiency over 10,000 cycles at 20 C [66].

4. Hierarchically Porous NVPF Cathodes

The introduction of fluorene to NVP has emerged as highly promising for SIBs [67]. Fluorene incorporated into the NVP framework effectively increases the voltage due to the enhanced ionicity it brings. The larger ionicity of the F–V bond and the inductive effect of

(PO₄)₃ further enhance the potential of NVPF cathodes [68]. The greater electronegativity of F leads to stronger ionic bonds, resulting in a higher specific capacity in NVPF compared to other polyanionic cathodes. The multivalent nature of V leads to the formation of a V³⁺/V⁵⁺ redox pair. The inductive effect of the PO₄ group on the V³⁺/V⁵⁺ redox pair increases the potential and working voltage of NVPF cathodes. Based on the crystal structure, several NVPF cathode materials have been developed, including Na₃V₂(PO₄)₂F₃ (tetragonal), Na₃V₂O₂(PO₄)₂F (sandwich), and Na_{1.5}VPO_{4.8}F_{0.7} (pseudo-layered). The theoretical specific capacities of NaVPO₄F and Na₃V₂(PO₄)₂F₃ are 143 mAh/g and 128 mAh/g, respectively. Na₃V₂(PO₄)₂F₃ possesses a stable crystal structure with a fast 3D tunnel for ion transport, high working potential (3.9 V), and energy density (507 Wh/kg). The highly electronegative F anion and the P–O covalent bond in PO₄ create a stable 3D structure with considerable open space. However, the electron transfer in the V–O–P–O–V bonds is slower, leading to decreased electronic conductivity in NVPF cathodes. Additionally, the large size and isolation of PO₄ result in the lower capacity and electrical conductivity of NVPF. As a result, the actual specific capacity and rate performance of NVPF cathodes are often observed to be lower. Various strategies have been developed to improve the electrochemical performance by increasing the electronic conductivity and accelerating the Na⁺ diffusion. Preparation of hierarchically porous NVPF cathode materials is considered a useful strategy for increasing the number of active sites and shortening the length of ion diffusion. Hydrothermal, solvothermal, spray pyrolysis, solid-state synthesis, and microwave-assisted refluxing have been employed for preparing NVPF HPMs.

4.1. NVPF Cathodes by Hydrothermal Method

The hydrothermal method is utilized for the preparation of several NVPF HPMs, including graphene–NVPF composites, multi-walled carbon nanotube–NVPF composites, NVPF–carbon core-shell cathodes, and NVPF with varying amounts of carbon coating. To achieve high-voltage cathodes and gain insights into the structure and properties of the NVPF family of compounds, Serras et al. synthesized a series of NVPF using the hydrothermal method. Various samples were prepared by adjusting the quantity and type of the carbon. For synthesis, either active carbon or S-black carbon was blended with V₂O₅ and NH₄H₂PO₄, and then subjected to annealing twice at 300 and 850 °C in an N₂ atmosphere. Subsequently, NaF was added to this blend and maintained under hydrothermal conditions (170 °C for 48 h). These samples exhibited a mixed valence state (V³⁺/V⁴⁺), with the formula Na₃V₂O_{2x}(PO₄)₂F_{3-2x} (0 ≤ x < 1). Particles with diverse shapes and sizes, around 1 μm in size, were obtained, and the type of the carbon did not limit the particle growth. The highest specific capacity value obtained was approximately 100 mA h/g, equivalent to about 80% of the theoretical value. Furthermore, the highest cyclic stability of 98% was observed after 30 cycles [69]. The cathode materials prepared using the hydrothermal method, along with their preparation conditions and electrochemical performance, are provided in Table 5.

Under oxidizing conditions, particularly in a hydrothermal atmosphere, NVPF is known to be unstable. Carbon coating was utilized to enhance its stability. NVPF exists in mixed valence states of V, specifically Na₃(VO)₂(PO₄)₂F (V⁴⁺) and Na₃V₂(PO₄)₂F₃ (V³⁺). The ratio of V³⁺/V⁴⁺ states in NVPF was largely determined by the amount of carbon present during synthesis. The V⁴⁺ state resulted when there was no carbon in the sample, while the V³⁺ state was obtained regardless of the carbon content. NVPF with a mixed V³⁺/V⁴⁺ state was considered an efficient cathode material. Serras et al. synthesized Na₃V₂O_{2x}(PO₄)₂F_{3-2x} from a ceramic precursor and evaluated the role of the carbon content in stability. Initially, NH₄H₂PO₄ and Kejten black (carbon source) were mixed in an agate mortar and annealed twice at 300 and 850 °C. Then, NaF was added to this mixture at a 3.3/1 molar proportion and subjected to hydrothermal treatment at 170 °C for 65 h. Combined X-ray diffraction and X-ray absorption spectroscopy analyses confirmed that a moderate carbon content (~6 wt.%) was suitable for obtaining NVPF with mixed V³⁺/V⁴⁺

valence states. These findings are crucial for understanding the mechanism of sodium extraction/insertion and for developing the optimal NVPF cathode material for SIBs [70].

Kumar et al. prepared a high-voltage insertion cathode by fabricating a composite of multi-walled carbon nanotubes (MWCNTs) and NVPF. Initially, a solid-state reaction was conducted by annealing V_2O_5 , $NH_4H_2PO_4$, and MWCNTs in an N_2 atmosphere twice, at 300 °C and 850 °C. Subsequently, this mixture was combined with NaF and subjected to mild hydrothermal treatment at 170 °C for 72 h. In an aqueous medium, MWCNTs prevented the complete oxidation of V^{3+} to V^{4+} . The authors reported, for the first time, the reversible electrochemical activity of NVPF. The observed reversible capacity was 65 mAh/g, with a stability of 75% over 400 cycles, both measured at a rate of 10 C. In aqueous electrolytes, NVPF-MWCNT remained stable for up to 1100 cycles. This composite cathode exhibited high energy density (84 Wh/kg) and a high full-cell voltage (1.7 V). The mixed valence polyanion property of this composite shows promise for developing both aqueous and non-aqueous low-cost SIBs [71].

Carbon coating on NVPF emerges as a promising solution to meet the performance requirements for high-power applications of SIBs, facilitating rapid ion diffusion and electron transport capability. Various carbon materials, such as graphene, carbon fibers, tubes, and particles, have been employed for this purpose. While NVPF–carbon core-shell materials have been suggested as a viable option for enhancing SIB performance by improving the conductivity, the multilayer structure poses challenges, particularly in ensuring direct contact with conductive components like graphene. A nanoscale 3D electrode architecture comprising highly conductive channels has proven more efficient than core-shell materials. Initially, a composite of NVPF–graphene (NVPF/G) was prepared using the hydrothermal method (180 °C for 24 h). The resulting brown powder was dissolved in water with the required amount of sucrose. This mixture was heated with stirring until drying, followed by grinding and annealing (550 °C for 1 h) in an argon atmosphere to form NVPF nanocubes. These nanocubes were embedded in graphene sheets and enveloped by sucrose-derived carbon. The carbon-wrapped NVPF/G cathode exhibited a high reversible capacity of 137.5 mA h/g and 98.9% stability over 40 cycles. The combination of NVPF with a carbon network and graphene sheets created an open and highly conductive structure capable of efficiently transporting Na^+ ions and electrons [72].

Through the hydrothermal method, Guo et al. synthesized NVPF containing uniform and carbon-free nano-tetraprisms. In the typical synthesis process, a glaucous suspension of V_2O_5 and $H_2C_2O_4$ (in a 1:3 molar ratio) was first prepared. Then, a stoichiometric quantity of $NH_4H_2PO_4$ and NaF was added to the suspension, and the pH was adjusted to 7.00 using ammonia. The resulting greenish mixture underwent hydrothermal treatment at 170 °C for 12 h. The obtained NVPF nano-tetraprisms had a length of 400 nm and a width of 200 nm. This cathode exhibited a discharge plateau at 4.01 and 3.60 V. The specific capacity observed (127.8 mA h/g) was very close to the theoretical value (130 mA h/g). The energy density of this cathode material (486 Wh/kg) was 23% higher than the theoretical value (394 Wh/kg) reported for $Na_3V_2(PO_4)_3$ [73].

Zhu et al. developed an NVPF–graphene composite through a hydrothermal method, integrating graphene, synthesized via the Hummers method, with NVPF precursors [74]. This synthesis involved treating the mixture in an autoclave at 180 °C for 12 h. The resulting NVPF particles formed an interconnected network with graphene, enhancing the composite's properties. This approach provides an alternative to traditional synthesis methods. To illustrate, Figure 6a depicts the solid-state high-temperature synthesis method for micro-sized NVPF, while Figure 6b showcases the solvothermal approach at low temperatures for producing nano-sized NVPF without a carbon coating. Moreover, Figure 6c illustrates the hydrothermal method at low temperatures for preparing NVPF \subset GN, highlighting its effective mixed-conducting networks.

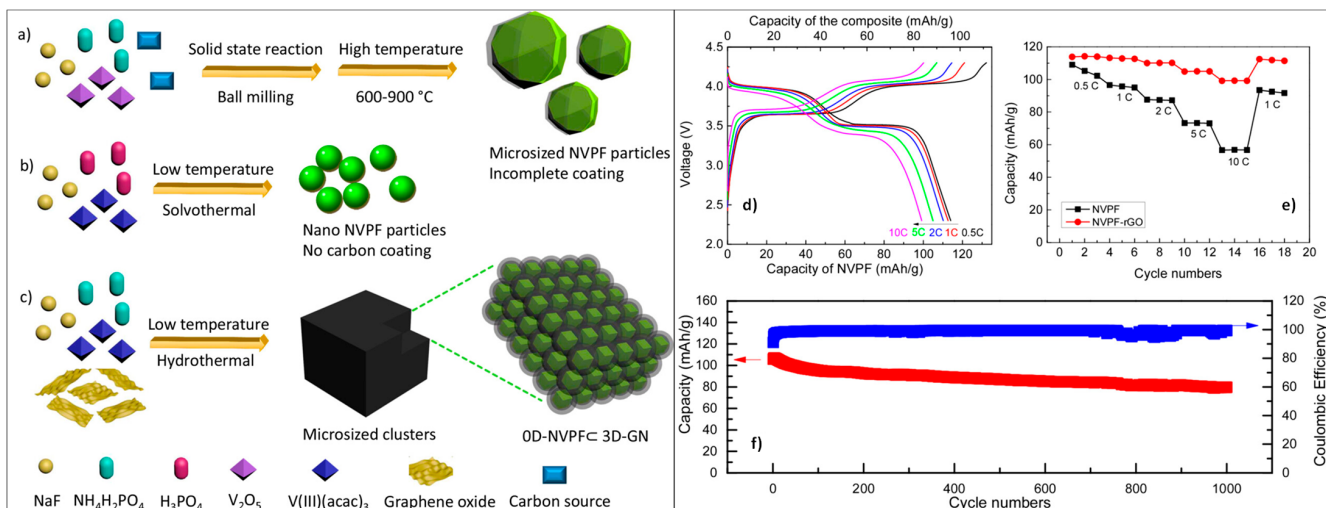


Figure 6. Diagram illustrating various synthetic methods for comparison. (a) Traditional solid-state high-temperature synthesis method for micro-sized NVPF. (b) Solvothermal approach at low temperatures for producing nano-sized NVPF without carbon coating. (c) Hydrothermal method at low temperatures for preparing NVPF \subset GN with effective mixed-conducting networks. (d) Galvanostatic charge–discharge profiles of NVPF \subset GN cathodes at different current densities. Capacities are referenced to the composite mass, with the upper and lower x-axis indicating the mass of NVPF. (e) Comparison of rate capability between NVPF and NVPF \subset GN. (f) Long-term cycling stability of NVPF \subset GN demonstrated over 1000 cycles at 10 C [74].

Table 5. NVPF-based cathode material preparation conditions and electrochemical performance using the hydrothermal method.

S. No.	Cathode Material	Method and Conditions	Modification	Specific Capacity (mA h/g) Current Rate (C)	% Stability/ Number of Cycles—Current Rate (C)	Reference
1	Na ₃ V ₂ O _{2x} (PO ₄) ₂ F _{3-2x}	Solid-state annealing (300 and 850 °C/N ₂)—Hydrothermal (170 °C/48 h)	Carbon composite	100—1 C	98/30—1 C	[69]
2	Na ₃ V ₂ O _{2x} (PO ₄) ₂ F _{3-2x}	Solid-state sintering (300 and 850 °C/N ₂)—Hydrothermal (170 °C/65 h)	Carbon coating	98—1 C	-	[70]
3	Na ₃ V ₂ O _{2x} (PO ₄) ₂ F _{3-2x}	[V(PO ₃) ₃]n/MWCNT by solid-state sintering (300 °C/N ₂ ; 850 °C/N ₂)—Hydrothermal (170 °C/72 h)	MWCNT composite	~65—10 C	75/400—10 C	[71]
4	Na ₃ V ₂ O ₂ (PO ₄) ₂ F	Hydrothermal (180 °C/24 h)—Sintering (550 °C/1 h/Ar)	Carbon coating	113.2—1 C	98.9/40—1 C	[72]
5	Na ₃ V ₂ (PO ₄) ₂ O ₂ F	Hydrothermal (170 °C/12 h)	Carbon-free nano-tetraprism composite	127.8—0.1 C	80.9/2000—20 C	[73]
6	Na ₃ V ₂ (PO ₄) ₂ F ₃	Hydrothermal (180 °C/12 h)	Graphene coating	99—10 C	75/1000—10 C	[75]

The synthesized NVPF \subset GN composite exhibited promising electrochemical performance. The galvanostatic charge–discharge profiles of the NVPF \subset GN cathode at different

current densities are shown in Figure 6d. The capacities are referenced to the composite mass, with the upper and lower x-axis indicating the mass of NVPF. Figure 6e provides a comparison of the rate capability between NVPF and NVPF \subset GN, indicating the enhanced performance of the composite. Furthermore, Figure 6f demonstrates the long-term cycling stability of NVPF \subset GN, which was maintained over 1000 cycles at 10 C. The energy density of the NVPF-graphene composite was measured at 348 Wh/kg. After 1000 cycles, the specific capacity remained at 80 mAh/g, retaining 75% of its initial value, with a Coulombic efficiency of approximately 99.3%. This composite presents itself as a cost-effective and high-energy cathode option for SIBs [74].

4.2. NVPF Cathodes by Solvothermal Method

Solvothermal synthesis is akin to the hydrothermal method, with the distinction that an organic solvent replaces water, either fully or partially, as the reaction medium. The choice of solvent depends on the nature of the reactants and the desired properties of the resulting products, such as the morphology [75]. Common organic solvents used in solvothermal synthesis include dimethylformamide (DMF), ethylene glycol, ethanol, diethylformamide, and acetonitrile [76]. In a typical solvothermal process for preparing nanostructured materials, the stoichiometric quantities of precursors or starting materials are mixed in the selected solvent medium, with or without templates, and then treated in a sealed autoclave at temperatures ranging from 100 to 250 °C for the required duration [77]. Heating above the boiling point of the solvent increases the solubility of the reactants and facilitates the reaction. Throughout the reaction, the formation of nuclei, crystal growth, and crystal formation occur in a sequential manner [78]. The solvothermal method finds application in the preparation of flexible, carbon-coated, and high-surface-area NVPF HPMs. The cathode materials prepared using the hydrothermal method, along with their preparation conditions and electrochemical performance, are provided in Table 6.

Table 6. NVPF-based cathode material preparation conditions and electrochemical performance using the solvothermal method.

S. No.	Cathode Material	Method and Conditions	Modification	Specific Capacity (mA h/g—Current Rate (C))	% Stability/Number of Cycles—Current Rate (C)	Reference
1	Na ₃ V ₂ O ₂ (PO ₄) ₂ F	Solvothermal (180 for 12 to 24 h)	Carbon/RGO composite	120—C/20	91.4/200—C/10	[79]
2	(VO _{1-x} PO ₄) ₂ F _{1+2x}	Solvothermal (60–120 °C/10 h)—Sintering (750 °C/1.5 h/Air)	Carbon coating	112—0.2 C (C/5)	90//1200—2 C	[80]
3	Na ₃ (VO) ₂ (PO ₄) ₂ F	Solvothermal (180 °C/20 h)—Sintering (400 °C/35 min/Ar)	GQD coated	70—45 C	81/2000—45 C	[81]
4	Na ₃ V ₂ O ₂ (PO ₄) ₂ F	Solvothermal (180 °C/24 h)—Sintering (550 °C/1 h/Ar)	Graphene Composite	135.8—0.1 C	96.8/50—2 C	[82]
5	Na ₃ (VO) ₂ (PO ₄) ₂ F	Two-step solvothermal synthesis (170 °C/3 h; 180 °C/6 h)	Grown on graphene foam	130—1 C	90/10,000—50 C	[83]
6	Na ₃ V ₂ (PO ₄) ₂ O ₂ F	Solvothermal (180 °C/24 h)	Carbon coating	85.4—50 C	62.2/2000—20 C	[84]
7	Na ₃ V ₂ (PO ₄) ₂ F ₃	CQD by hydrothermal (160 °C/3 h)—Solvothermal (170 °C/9 h)—Sintering (480 °C/8 h)	CQD coating	105.1—20 C	90.2/6000—30 C	[85]

Table 6. Cont.

S. No.	Cathode Material	Method and Conditions	Modification	Specific Capacity (mA h/g—Current Rate (C))	% Stability/Number of Cycles—Current Rate (C)	Reference
8	Na ₃ V ₂ (PO ₄) ₂ F ₃	Solvothermal (180 °C/20 h)—Sintering (500 °C/4 h/N ₂)	C composite/RGO	95—2 C	78.2/1500—5 C	[86]
9	Na ₃ V ₂ (PO ₄) ₂ F ₃	Solvothermal (170 °C/9 h)—Sintering (480 °C/6 h)—Wet chemical (100 °C/12 h)—Sintering (500 °C/3 h)	Carbon coating	116.2—0.2 C	85/2000—5 C	[87]

An issue in the synthesis of NVPF arises due to the presence of fluorine, which can react with glass and ceramic materials, leading to contamination. Consequently, solid-state reactions must be conducted in expensive tubular reactors made of platinum or gold. However, Xu et al. addressed this challenge by preparing Na₃V₂O₂(PO₄)₂F/RGO composites via a single-step hydrothermal method. In their approach, a N,N'-dimethylformamide (DMF) dispersion of graphene oxide (GO) was mixed with aqueous solutions of NH₄VO₃ and NaF. Then, (NH₄)₂HPO₄ was added dropwise to the mixture, which was subsequently subjected to solvothermal treatment at 180 °C for 12–24 h. The resulting samples were collected by filtration and dried in air at 120 °C for 12 h. This process yielded nanocubes of NVPF-RGO with a unique sandwich structure, where the NVPF nanoparticles were trapped between RGO sheets and assembled into a compact sandwich structure. This material exhibited a high reversible capacity of 120 mA h/g and retained 91.4% of its capacity after 200 cycles. Anchoring on electrically conducting RGO sheets enhanced the utilization of electrochemically active NVPF. The reported method offers significant advantages—it is simple, inexpensive, and operates at a low temperature compared to the multi-step solid-state firing method [79].

To reduce the energy and cost consumption, Qi et al. developed a low-temperature solvothermal route, operating between 60 °C and 120 °C for 10 h. Prior to solvothermal treatment, the precursor solution underwent high-energy ball milling and was heat-treated at 750 °C for 1.5 h in air. No organic ligands or surfactants were used in the process, and the reaction occurred spontaneously, even at room temperature, resulting in a high yield of 96.5%. The particle sizes of the NVPF ranged from 50 to 100 nm. A representative sample exhibited a specific capacity of 112 mAh/g, and remarkable cyclic stability was reported, with 90% retention over 1200 cycles. This single-step solvothermal synthesis method is anticipated to have the potential to be used as a general synthesis route for NVPF cathodes [80].

Deng et al. investigated strategies to improve the cyclic stability of NVPF, focusing on a hierarchical coating approach. This approach included three key strategies: (i) controlled growth of NVPF crystals in preferred [001] orientation; (ii) coating the NVPF surface with graphene quantum dots (GQD); and (iii) coating carbon on the NVPF surface decorated with QD. Through this strategy, NVPG hierarchically coated with GQD and an amorphous carbon layer were obtained. This hybrid material delivered a specific capacity of 70 mAh/g and exhibited 81% cyclic stability after 2000 cycles. Thus, this material configuration is considered an effective strategy for achieving high-power, long-life NVPF cathodes [81].

Jin et al. prepared an NVPF–carbon–graphene composite using the solvothermal method. In this composite, NVPF cubes with multiple layers were stacked between graphene sheets, while homogeneous and nanoporous carbon with a thickness of 5 nm was coated on the NVPF, resulting in a 3D structure. This composite cathode exhibited a reversible capacity of 135.8 mAh/g, with 96.8% capacity retention after 50 cycles. In contrast, the cyclic stability of NVPF alone and NVPF–graphene was 50.2% and 85.8%,

respectively. In the NVPF-graphene composite, the NVPF particles were located between graphene sheets, leading to poor conductivity. However, the presence of porous carbon in the integrated 3D structure increased the conductivity and cyclic stability [82].

To address the structural stability and electrical contact issues associated with flexible cathodes based on graphene and carbon nanotubes, Chao et al. developed single-crystalline NVPF. They utilized a VO₂ array as a seed layer and employed freestanding graphene foam along with 3D VO₂ nanosheets and NVPF precursors to prepare the single-crystalline NVPF via solvothermal treatment and annealing. The flexible and lightweight graphene foam served as the backbone for this cathode. It exhibited a specific capacity of 130 mA h/g and remarkable durability, lasting through 10,000 cycles. The small volume change, array morphology, and rapid ion transport contributed to its high rate capability [83].

NVPF, a sodium-ion superionic conductor (NASICON)-based electrode material, is gaining attention as a potential cathode for SIBs due to its high Na⁺ mobility and structural diversity. NVP with a high specific surface area (greater than 100 m²/g) is preferred, as large electrodes are not conducive to efficient electron transfer and electrolyte transportation. Cathode materials with structures capable of enhancing the electrolyte accessibility are particularly promising. In pursuit of NVP with a greater surface area, Zhao et al. reported a single-step, template-free synthesis strategy for hierarchically porous NVP hollow nanospheres (HPNs). Through a three-step solution-mixing procedure incorporating NaF, NH₄H₂PO₄, V(IV) acetylacetone (VO(acac)₂), and dimethylformamide (DMF), HPNs were obtained via solvothermal treatment (180 °C, 24 h). These HPNs comprised high-crystalline nanoparticles on the shell, featuring a spacious inner nanospace and numerous pores. This hierarchical structure formed via an Ostwald-ripening mechanism during the solvothermal process. The HPNs exhibited a reversible capacity of 127.1 mAh/g, exceptional stability over 2000 charge/discharge cycles, with cycling stability amounting to 99.077%. This outstanding performance is attributed to several factors, including the reduction of the Na⁺ migration distance by nanosized HPNs, barrier-free pathways, accommodation of volume changes during Na⁺ migration, and effective electrode-electrolyte contact. These results surpass those reported for other NVP-based materials. The use of a low-temperature solution-processing method offers advantages for the facile and economical production of NVP-based cathodes, making it suitable for large-scale industrial production of SIBs [84].

GQDs have demonstrated their capability to prevent the agglomeration of NVPF and enhance electronic conductivity. Liu et al. developed hierarchically porous NVPF/CQD microspheres. CQD was prepared by treating sucrose under hydrothermal conditions (160 °C for 3 h). The sucrose-derived CQD in an aqueous medium was mixed with NVPF precursors and poly(vinylpyrrolidone) dissolved in ethanol. This mixture underwent solvothermal treatment in an autoclave (170 °C for 9 h). The resulting powder was then sintered at 480 °C for 8 h under Ar flow. The NVPF/CQD composite exhibited a discharge capacity of 105.1 mAh/g and 92.2% stability after 6000 cycles. The exceptional capacity and stability were attributed to the 3D hierarchical porous structure of NVPF/CQD, which provided a short Na⁺ diffusion pathway, improved electron transfer, and enhanced volumetric energy density. The NVPF/CQD cathode shows promise for practical applications [85].

Following the strategy of morphology control and carbon coating, Du et al. prepared NVPF/C/RGO microspheres via a solvothermal method. Initially, they synthesized NVPF/C by subjecting the NVPF precursors, glucose, and a tetraethylene glycol mixture to solvothermal treatment (180 °C for 20 h). The solvothermal product was then calcined (500 °C for 4 h) in an N₂ atmosphere. Next, NVPF/C was mixed with GO dispersion under ultrasonic conditions and subjected to identical calcination as NVPF/C. The optimized NVPF/C/RGO exhibited a discharge capacity of 118 mA h/g and 51.7% stability after 1500 cycles. In the NVPF/C/RGO composite, mesoporous nanosheets were assembled into microspheres, favoring the shortening of the ion and electron diffusion pathways. The RGO coating improved the interfacial conductivity and restricted the undesirable electrode/electrolyte side reactions [86].

Liang et al. synthesized multi-clustered hierarchically porous NVPF microspheres coated with nitrogen-rich carbon resulting from the carbonization of PAN. They employed a combination of solvothermal processing, wet chemical polymer coating, and a calcination process. The preparation process for NVPF-H@cPAN is illustrated in Figure 7a', emphasizing the synthesis methodology. Initially, the NVPF precursors underwent a solvothermal process, with ethylene glycol serving as the solvent. Subsequently, the NVPF obtained from this process was stirred with a PVP solution and sintered to produce hierarchically porous and multi-clustered NVPF microspheres. Figure 7a–e shows the evaluation of the electrochemical performance of the NVPF-H@cPAN || CHC full cells. This cathode demonstrated a high reversible capacity of 116.2 mAh/g and 85% cyclic stability over 2000 cycles. The structural regulation of NVPF microspheres in a multi-cluster enhanced the rate of Na^+ diffusion and the extent of carbon coating. The multi-cluster structure reduced the length of the diffusion pathway for ions and electrons, creating multiple active sites. Consequently, the electrochemical performance of hierarchically porous and multi-clustered NVPF microspheres surpassed that of bulk NVPF [87].

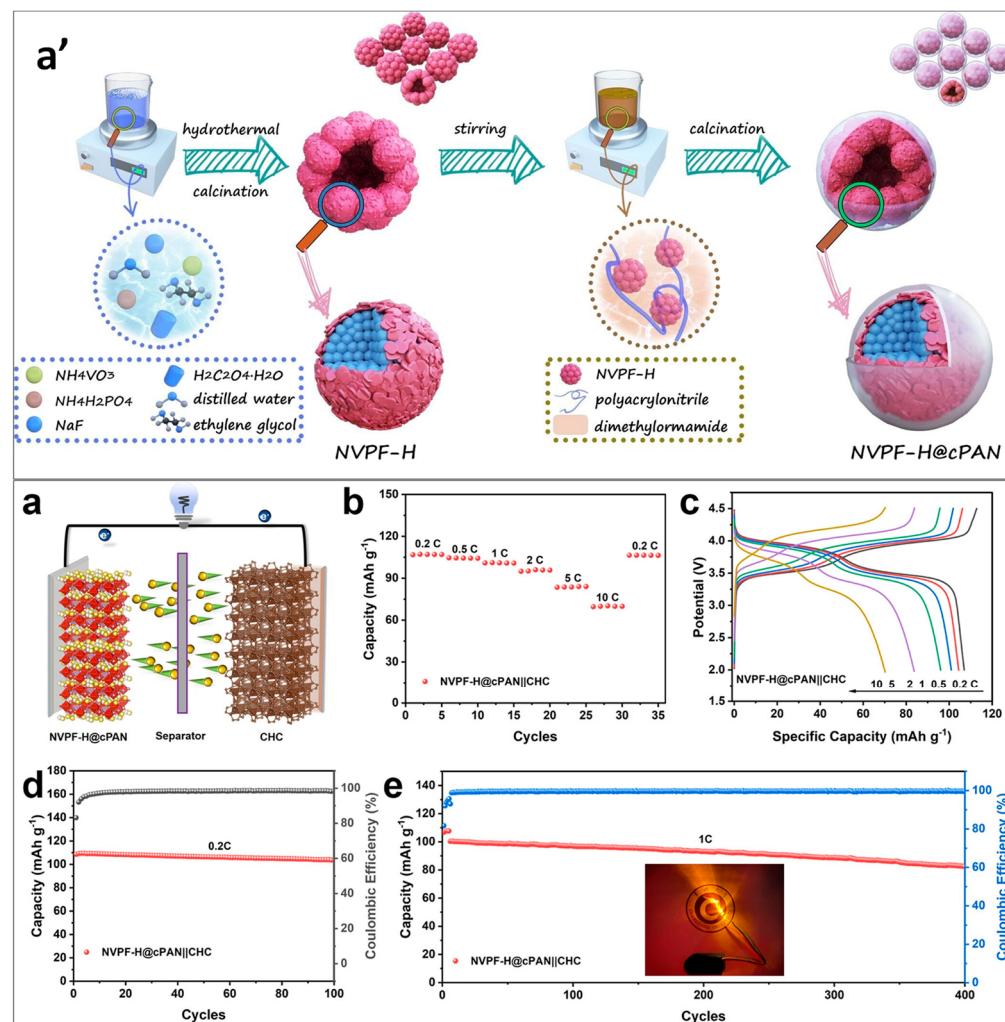


Figure 7. (a') Illustration depicting the preparation process for NVPF-H@cPAN. (a) Schematic representation of the NVPF-H@cPAN || CHC sodium-ion full cell. Evaluation of electrochemical performance of the NVPF-H@cPAN || CHC full cells. (b) Rate capacity assessed at various rates. (c) Charge and discharge curves observed at different rates. Cycling capacity demonstrated at: (d) 0.2 C and (e) 1 C. The inset showcases an LED lamp illuminated by the full cell [87].

4.3. NVPF Cathodes by Spray Pyrolysis

Spray pyrolysis is a cost-effective and simple technique employed for forming thin films from a solution formulation containing precursors. In this process, the solution formulation is atomized into droplets, which are then deposited onto a substrate heated to an elevated temperature. Here, the precursors completely solidify into particles of the desired size or form a film with the desired thickness.

To meet the performance requirements for practical applications, Yin et al. prepared graphene-encapsulated three-dimensional NVPF nanoparticles using the spray-drying method. Figure 8a' depicts the synthetic procedure for the NVOPF/rGO microsphere composite. They created a solution composite of NVPF and graphene oxide, which was then spray-dried. After calcination at 500 °C for 5 h, the resulting NVPG/GO microspheres transformed into NVPF/RGO composites. These composites featured well-crystallized NVPF nanoparticles encapsulated within the three-dimensional framework of flexible rGO sheets. Assessment of the electrochemical properties of NVOPF/rGO within the potential window ranging from 2.5 to 4.5 V is shown in Figure 8a–e. NVPG/RGO exhibited a reversible capacity of 127.2 mAh/g and demonstrated 83.4% cycling performance after 2000 cycles. The 3D RGO skeleton served as an electronic conduction framework, facilitating effective electron conduction while preserving the integrity of the morphology during repeated charging and discharging processes [88].

Ultrasonic spray pyrolysis (USP) proves valuable for the single-step and template-free synthesis of hollow NVPF structures. Langrock et al. synthesized carbon-coated hollow NVPF spheres (NVPF/C) using this method. They sprayed an aqueous precursor mixture containing NaF, NaNO₃, iron nitrate nonahydrate, phosphoric acid, and sucrose at 500 °C under an N₂ atmosphere. This process yielded NVPF/C spheres with a diameter of 500 nm and a wall thickness of 80 nm. Nanopores across the walls of the NVPF/C spheres facilitated electrochemical reactions both outside and inside the spheres. The specific capacity reached 89 mAh/g, with 80% capacity retention after 750 cycles. The space within the nanopores and micro-cavities in the NVPF/C spheres accommodated volume changes, leading to improved cyclic stability [89].

4.4. NVPF Cathodes by Solid-State Synthesis

Ball milling-assisted solid-state synthesis has been employed to prepare carbon-coated NVPF and to control the oxidation state of vanadium and fluorine during NVPF formation. The carbon coating on NVPF has been identified as an effective method for enhancing its performance. Carbon sources such as sucrose and ascorbic acid have been found to be useful for both carbon coating and limiting the growth of NVPF particles. In the solid-state reaction method, NaF, NaHCO₃, FeC₂O₄·2H₂O, NH₄H₂PO₄, and ascorbic acid are mixed using ball milling and then subjected to initial annealing at 300 °C for 2 h. The sample is subsequently ground and heated to either 600 or 650 °C for 10 h, with both annealing steps performed under an N₂ atmosphere. This process results in the formation of carbon-coated NVPF with particle sizes ranging from 50 to 500 nm. The NVPF with 1.3 wt.% carbon coating exhibits a specific capacity of 110 mAh/g, with 75% of the initial capacity retained after 20 cycles [90]. The cathode materials prepared using solid-state synthesis, along with their preparation conditions and electrochemical performance, are provided in Table 7.

Park et al. synthesized a series of solid solutions of NVPF via solid-state reactions, employing the stoichiometric quantities of VOPO₄, VPO₄, NaF, and Na₂CO₃. These precursors underwent high-energy ball milling at 300 rpm for 24 h, followed by heat treatment in an Ar atmosphere at 850 °C for 2 h. Rather than controlling the quantity of the precursors, the oxidation states of vanadium and fluorine were managed. During cycling, this cathode demonstrated an exceptionally small volume change of approximately 2%. The NVPF sample, Nay(VO_{1-x}PO₄)₂F_{1+2x}, exhibited the highest energy density of around 520 Wh/kg. These cathodes possess properties such as high energy density and ultrahigh stability, rendering them promising candidates for the fabrication of inexpensive and high-performance SIBs [91].

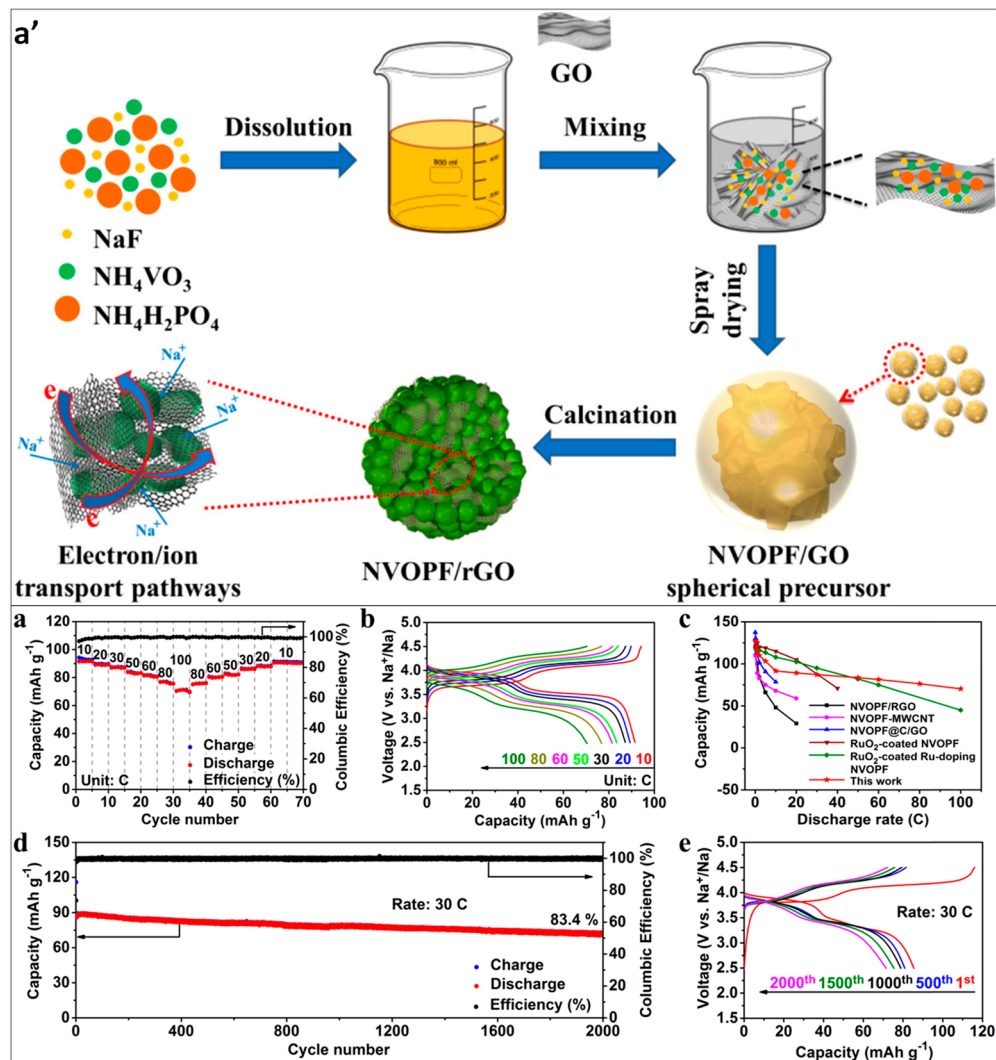


Figure 8. (a') Depiction of the synthetic procedure for the NVOPF/rGO microsphere composite. Assessment of the electrochemical properties of NVOPF/rGO within the potential window ranging from 2.5 to 4.5 V. (a,b) Evaluation of high-rate performance alongside corresponding charge–discharge curves. (c) Comparative analysis of rate performance with recent literature findings. (d) Demonstration of long-term cycle performance at 30 C. (e) Presentation of corresponding charge–discharge curves across different cycles [88].

Deng et al. utilized a ball-milling method to prepare hierarchical porous Na₂FePO₄F coated with green organic carbon to address the poor conductivity of Na₂FePO₄F, thereby improving the cycling stability and rate capability. Vitamin C served as the carbon source in this process. Stoichiometric quantities of NaCH₃COO, Fe(CH₃COO)₂, and NH₄H₂PO₄ were subjected to ball milling at 400 rpm for 2 h. The resulting mixture underwent drying and two-stage calcination: first at 350 °C for 2 h and then at 600 °C for 6 h, both under Ar flow. For the preparation of carbon-coated Na₂FePO₄F, vitamin C (20%) was added after the first calcination step. The introduction of the carbon source led to the formation of a hierarchical pore structure with mesopores (3.4 nm) and macropores (17 nm), unlike the carbon-free Na₂FePO₄F, which only had pores. The specific surface area increased significantly from approximately 5.4 m²/g for neat Na₂FePO₄F to approximately 31.9 m²/g for carbon-coated Na₂FePO₄F, attributed to the smaller particle size and higher pore volume. The carbon-coated Na₂FePO₄F cathode exhibited a high specific capacity of 66.8 mAh/g and superior cycling stability, retaining 84.7% of its capacity after 1000 cycles [92].

Table 7. NVPF-based cathode material preparation conditions and electrochemical performance using solid-state synthesis.

S. No.	Cathode Material	Method and Conditions	Modification	Specific Capacity (mA h/g—Current Rate (C))	% Stability/Number of Cycles—Current Rate (C)	Reference
1	Na ₃ FePO ₄ F	Ball milling and two-step sintering (300 °C/2 h/N ₂ ; 600 or 650/10 h/N ₂)	Carbon coating	110—1/20 C	75/20—1/20 C	[90]
2	Na ₃ (VO _{1-x} PO ₄) ₂ F _{1+2x}	High-energy ball milling—Sintering (850 °C/2 h/Ar)	Varying VO and F content	120 to 130—C/10	90/150—C/2	[91]
3	Na ₂ FePO ₄ F	High-energy ball milling—Sintering (350 °C/2 h/Ar; 600 °C/6 h/Ar)	Carbon coating	117—0.1 C	85/1000—4 C	[92]

4.5. NVPF Cathodes by Microwave-Assisted Refluxing

Microwave-assisted refluxing is a non-classical methodology where molecules are heated directly using microwaves, in contrast to conventional methods such as Bunsen burners, oil baths, or electrical heating. This results in a naturally rapid and efficient reaction process, significantly reducing the reaction times. Moreover, compared to traditional methods, microwave-assisted refluxing tends to produce lower amounts of chemical waste and hazards. This method has been utilized for obtaining plain carbon and graphene-coated NVPF HPMs, sometimes without the need for post-reaction sintering. The microwave-assisted approach offers several advantages, including the enhanced reaction kinetics, precise temperature control, and reduced energy consumption. Additionally, it allows for the synthesis of materials with tailored properties and controlled morphologies, making it a valuable technique in materials science and nanotechnology.

In order to circumvent the issues associated with the particle size increase and conductivity decrease resulting from the high-temperature annealing typically required after hydrothermal/solvothermal methods, Hou et al. developed a low-temperature rapid microwave-assisted refluxing method for the synthesis of NVPF. In this method, an aqueous solution containing vanadium (III) acetylacetone, ammonium dihydrogen phosphate, and sodium fluoride was mixed with tetraethylene glycol. The mixture was then refluxed at 120 °C for 1 h and subjected to a microwave digestion system at 220 °C. After 10 min, the solid content was collected and dried at 80 °C for 12 h. This procedure resulted in the formation of hierarchical self-assembly mulberry-shaped NVPF@C nano-composites, wherein the NVPF nanoparticles were encapsulated by carbon nanoparticles. The initial discharge capacity of NVPF@C was measured to be 127.9 mA h/g, with 82.1% of the initial capacity (88.1 mA h/g) retained after 2000 cycles. The carbon shell coating significantly contributed to the fast Na⁺ and electron transfer, while the self-assembled structure mitigated the voltage fading due to high structural stability. This proposed microwave-assisted refluxing method offers a new opportunity for the rapid preparation of high-performance NVPF cathodes for SIBs [93].

He et al. investigated the influence of a conductive reduced graphene oxide (rGO) coating on the electronic conductivity of hierarchically porous NVPF-RGO core-shell composites. Initially, the mixture of rGO and NVPF precursors underwent microwave-assisted hydrothermal treatment at 130 °C for 1 h. The solid residue obtained after hydrothermal treatment was freeze-dried, compressed into pellets, and calcined at temperatures ranging from 550 to 650 °C for 7 h under an argon atmosphere. Figure 9a depicts the formation mechanism. The resulting hierarchically porous NVPF-rGO composite exhibited highly graphitized rGO sheets conformally wrapped around the NVPF due to the absence of repulsive forces. Figure 9b–e represents the full-cell configuration and electrochemical

profiles. The NVPF-rGO cathode prepared at 600 °C demonstrated a discharge capacity of 105.9 mAh/g, with 99.1% capacity retention over 200 cycles, and a rate performance of 90.6 mAh/g. The robust rGO coating and synergistic core-shell morphology enhanced the electronic conductivity and overall electrochemical properties, making them suitable for practical applications [94].

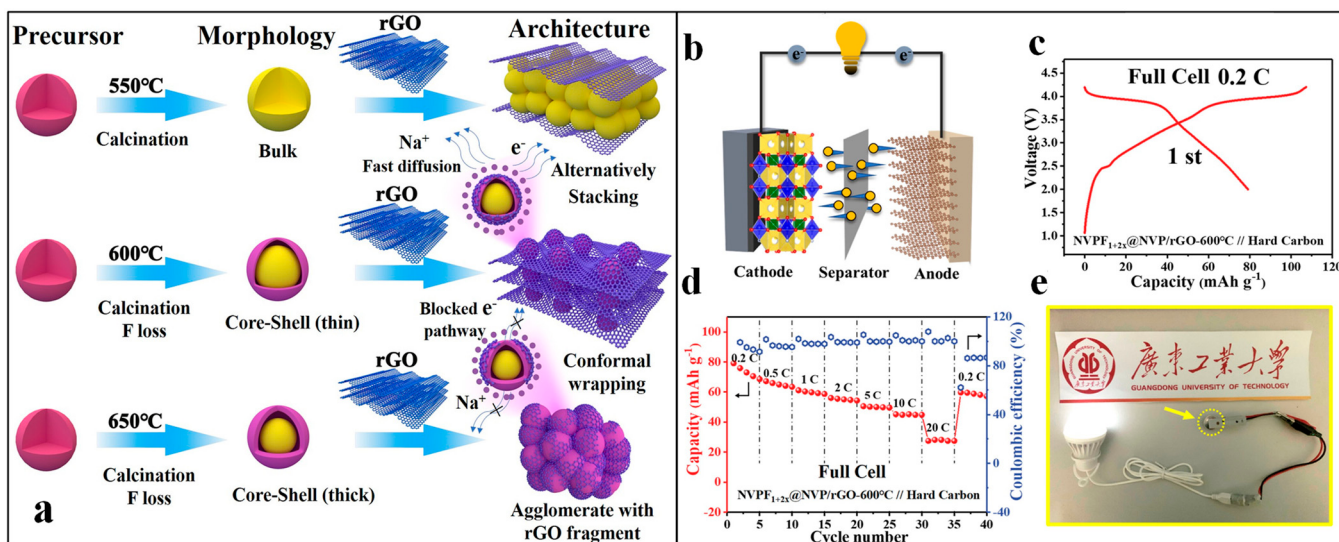


Figure 9. (a) Diagram depicting the formation mechanism of NVPF_{1+2x}/rGO-550 °C, NVPF_{1+2x}@NVP/rGO-600 °C, and NVPF_{1+2x}@NVP/rGO-650 °C composites at diverse calcination temperatures, showcasing different morphologies [60]. (b) Schematic representation of the full-cell configuration. (c) Initial charge/discharge profile. (d) Rate capability assessment at various C-rates. (e) Utilization of NVPF_{1+2x}@NVP/rGO || hard carbon (HC) sodium-ion full cell for powering light emitting diodes (LED) [94].

5. Hierarchically Porous V₂O₅ Cathodes

Multiple oxidation states of vanadium result in a two-dimensional (2D) layered structure with interfacial areas that facilitate the diffusion and storage of Na⁺. V₂O₅ cathodes exhibit the full theoretical capacity of 235 mA h/g and can maintain their integrity during Na⁺ insertion. However, commercial powder-type V₂O₅ cathodes often experience excessive volume expansion due to the large radius of the Na⁺ ions [95]. This intrinsic poor conductivity and volume expansion lead to lower overall electrochemical performance. To address these challenges, V₂O₅ cathodes with various morphologies have been synthesized. The ease of synthesizing V₂O₅ allows for precise control over the morphology. V₂O₅ cathode materials with large interlayer spacing have been developed, including V₂O₅ hollow nanospheres, V₂O₅ nanobelts, bilayered V₂O₅ nanobelts, and V₂O₅ xerogel. Among these, V₂O₅ HPMs cathodes, with their large storage area and 3D porous network, offer advantages over layered structures and contribute to achieving the desirable electrochemical performance. Hydrothermal and solvothermal methods have been employed to prepare hierarchical hollow nanospheres, microspheres, and organic–inorganic hybrids of V₂O₅ HPM cathodes. These techniques enable the synthesis of V₂O₅ cathode materials with tailored morphologies and structures, offering opportunities to enhance their electrochemical performance. The V₂O₅-based cathode materials' preparation conditions and electrochemical performance are provided in Table 8.

Table 8. V₂O₅-based cathode material preparation conditions and electrochemical performance.

S. No.	Cathode Material	Method and Conditions	Modification	Specific Capacity (mA h/g—Current Rate (C))	% Stability/Number of Cycles—Current Rate (C)	Reference
1	V ₂ O ₅	Solvothermal—Sintering solvothermal (140 °C/12 h)—Sintering (350 °C/2 h)	-	150.8 at 160 mA/g	94/100 at 160 mA/g	[19]
2	V ₂ O ₅	Hydrothermal (200 °C/24 h)—Sintering (350 °C/2 h/Air)	Unique hollow structure	254 mAh/g at 0.1 A/g	61/500 g at 0.5—2 A/g	[95]
3	V ₂ O ₅	Hydrothermal (120 °C/3 h)—Sintering (150 °C/30 min/Ar)	Benzoquinone-intercalated	252 at 0.05 A/g	90/2100 at 0.1 A/g	[96]

The layered V₂O₅ electrode, characterized by a large interlayer distance along the c-axis in its crystal structure, has shown potential for application in SIBs. The hollow sphere structure of the V₂O₅ electrode is recognized for its ability to withstand expansion and contraction during charge and discharge cycles. Su et al. synthesized hierarchical hollow nanospheres of V₂O₅ using a typical three-step synthesis procedure. Initially, a mixture of vanadyl acetylacetone, sulfuric acid, and ethanol was refluxed to produce VOSO₄. Subsequently, the VOSO₄ underwent treatment with sodium carbonate and acetylacetone, resulting in the formation of a blue–green VO-acetylacetone precipitate. This precipitate, along with polyvinylpyrrolidone, was introduced into ethylene glycol and heated with stirring until the mixture transformed into a transparent light-green solution. The solution was then subjected to heat treatment in an autoclave at 140 °C for 12 h. The solid residue obtained from this process was dried and sintered at 350 °C for 2 h to yield V₂O₅ nanocrystals characterized by predominant {110} crystalline facets and a hollow nanosphere morphology. When employed as a cathode in SIBs, these hierarchical hollow nanospheres exhibited a capacity of approximately 150.8 mAh/g at a current density of 160 mA/g. Following 100 cycles at 160 mA/g, a discharge capacity of 141 mAh/g was retained. The strain-accommodating nature of porous hollow nanospheres, combined with the two-dimensional diffusion pathway provided by the {110} crystalline facets of V₂O₅, facilitated the effective insertion and extraction of Na⁺ ions, thereby enhancing the electrochemical performance of the cathode material [19].

With the aim of enhancing the performance of V₂O₅-based 3D hierarchical structured cathodes, Zhao et al. synthesized hierarchical microspheres of V₂O₅ (HMs) formed by assembling nanosheets of V₂O₅ using a post-annealing method. Initially, VO₂ hollow microspheres were synthesized by treating an ethanolic solution of VOC₂O₄·5H₂O and aqueous citric acid under hydrothermal conditions (200 °C for 24 h). The resulting black VO₂ powder was then isolated and subjected to post-annealing at 350 °C for 2 h in an air atmosphere. Subsequently, the yellow V₂O₅ with a 3D hierarchical structure was obtained. This electrode material exhibited a high discharge capacity of 254 mA h g⁻¹ at 0.1 A g⁻¹, along with 61% capacity retention after 500 charge/discharge cycles. The improvement in the electrochemical properties was attributed to the 3D open structure of hierarchical structured V₂O₅, which facilitated fast Na⁺ ion diffusion and capacitive-dominant kinetics [95].

Low-molecular-weight and inexpensive quinone-based organic materials are considered promising for the next generation of cathodes for SIBs. Vanadium oxide serves as a protective material to prevent the dissolution of quinones in organic liquid electrolytes. Tang et al. studied the preparation of m-benzoquinone (mBQ)-intercalated V₂O₅ using a hydrothermal method to obtain an organic–inorganic hybrid cathode and to investigate

the influence of organic molecules on the structure of V_2O_5 . Porous and 3D hierarchical micro-flowers with large (001) lattice spacing (13.7 Å), crystalline vacancies, and disorders were obtained. The samples were annealed at 150 °C for 30 min under an argon atmosphere. The mBQ was well intercalated into the layered V_2O_5 , leading to the elongation of V–O bonds. Structural oxygen vacancies were found at V centers. The V–O–V bilayers were divided into two monolayers of V–O–V, with the (001) facet serving as the division plane. The initial capacity of this sample is 252 mAh/g (at 0.05 A/g), with a capacity retention of 90% over 2100 cycles. No phase change was witnessed. The redox-active mBQ provided additional capacity, and the anchoring effect of the V–O–V framework protected mBQ from leaching into the electrolyte [96].

6. Conclusions and Outlook

Most of the works reflect the fact that the preparation of NVP and NVPF has predominantly focused on improving the electrical and electronic conductivity. Carbon coating has been identified as the preferred method to achieve this objective. In the case of NVP HPMs, carbon coating primarily resulted from the controlled carbonization of organic materials, either as precursors or carbon sources. Doping with metal atoms and incorporating pre-synthesized carbon quantum dots were also utilized to a limited extent. Hierarchically porous structures were intrinsically formed through the carbonization of precursor products with network structures such as gels and micelles, while the use of porous carbon templates was rare. The carbon composite approach was equally employed in NVPF HPMs, where nanocarbon materials like reduced graphene oxide, multi-walled carbon nanotubes, and graphene foam were used to prepare NVPF–carbon composite HPMs. Additionally, NVPF HPMs were prepared with varying vanadium oxide and fluoride contents.

The sol-gel, hydrothermal, solid-state synthesis, and solution-blending and spraying methods were used to prepare high-performance NVP HPM cathodes. Sol-gel products underwent single or two-step sintering processes in an inert atmosphere (ranging from 350 to 800 °C in the presence of Ar and N₂). Carbon-coated NVPF HPM cathodes, prepared by Zhu et al. via a single-step sintering process at 800 °C in an Ar or N₂ atmosphere, exhibited greater cyclic stability (82.1% after 10,000 cycles) and reversible capacity (116.2 mA h/g). Hydrothermally prepared NVP HPMs also mostly underwent similar two-step sintering processes. Carbon-coated NVP HPMs, prepared by Ling et al. through a hydrothermal process (180 °C, 24 h) and a two-step sintering process (350 °C and 750 °C, Ar), showed 81.27% cyclic stability and a reversible capacity of 114.8 mA h/g. The single-step sintering process was mainly adopted for obtaining NVP HPMs via solution blending and spraying. The cyclic stability (90.9% after 10,000 cycles) and reversible capacity (102.31 mA h/g) were comparable to NVP HPMs prepared by the sol-gel and hydrothermal methods. In the solid-state synthesis of NVP HPMs, an Ar/H₂ atmosphere was used for the sintering process. Although a comparable reversible capacity was observed, the stability (82.1% over 5000 cycles) was lower than that of the sol-gel, hydrothermal, and solution methods.

The solvothermal method was extensively explored for preparing NVPF HPMs. Other methods employed included hydrothermal synthesis, microwave-assisted refluxing, and spray pyrolysis. Notably, a single-step hydrothermal process (170 °C for 12 h) produced highly efficient NVPF HPM cathodes, exhibiting a specific capacity of 127.8 mA h/g and retaining 80.9% stability after 2000 cycles, completely eliminating the need for a sintering step. This performance significantly surpassed that of NVPF HPMs obtained via single- or two-step high-temperature sintering through hydrothermal processes. Similarly, NVPF grown on graphene foam via a two-step solvothermal method (170 °C for 3 h; 180 °C for 6 h) demonstrated impressive performance with a specific capacity of 127.8 mA h/g and 90% stability, surpassing the aforementioned NVP and NVPF materials. Spray pyrolysis, which involves sintering at 400–500 °C for 5 h under Ar flow, yielded NVPF cathodes with a specific capacity of 127.2 mAh/g and 83.4% stability. Ball milling was predominantly employed for the solid-state synthesis of NVPF HPMs, typically followed by single- or two-step sintering. The highest performance achieved from the solid-state synthesis of

NVPF HPMs was an initial capacity of 117 mA h/g, with 85% capacity retention over 1000 cycles. Microwave-assisted refluxing emerged as a cost- and time-effective method, yielding NVPF HPM cathodes with performance comparable to spray pyrolysis. V_2O_5 HPMs were prepared using either hydrothermal or solvothermal methods. V_2O_5 HPMs derived from low-temperature sintering (150 °C for 30 min) via hydrothermal synthesis exhibited the highest reversible capacitance of 252 mA h/g, with a commendable stability of 90% over 2100 cycles.

The availability of low-cost raw materials for preparing SIB cathodes has been identified as crucial for replacing LIBs. Therefore, time- and cost-effective cathode preparation methods are potentially beneficial for further expanding the application of SIBs in industrial-scale energy storage and electric-powered vehicles. In terms of the performance (105.1 mAh/g and 92.2% stability after 6000 cycles) and preparation (solvothermal process—170 °C/9 h, and single-step sintering—480 °C/8 h/Ar), NVPF-CQD microspheres seem to have potential for practical application [85].

Notably, in order to widen the application of SIBs and move a step closer to commercialization, Rui et al. proposed NVP HPMs operable at low temperatures [8]. NVP HPMs were derived by a hydrothermal (180 °C for 16 h) process, forming aerogel by freeze-drying (48 h), and single-step sintering (750 °C for 16 h under Ar/H₂ (95:5)). At extremely low temperatures (−20 °C), this cathode exhibited reversible capacities of 105 mA h/g (at 0.2 C), excellent Na⁺ transport kinetics, and electrolyte absorption. In addition, NVPF with interfacial V–F–C bonding was also developed to build SIBs operable at even −40 °C. Hydrothermally synthesized (190 °C for 4 h) NVPF was used to make a composite with graphene by high-energy ball milling. The discharge capacity of 56 mAh/g (at 10 C) and 80% cyclic stability (over 500 cycles at 2 C) were observed at −40 °C [66]. An interfacial V–F–C bond was attributed to have caused the significant increase in the Na⁺ diffusion, electronic conductivity, compatibility at the interface, and workability at low temperature. Therefore, the recent investigation provides impetus for increasing the prospects of SIBs' practical application.

In conclusion, optimizing single- or multi-step hydrothermal or solvothermal methods can yield high-performance and cost-effective NVP, NVPF, and V_2O_5 HPM cathodes. These advancements are crucial for the development of sodium-ion batteries (SIBs) as a viable alternative to lithium-ion batteries, particularly in industrial-scale energy storage and electric-powered vehicles. Notably, carbon coating has been widely used to enhance the electrochemical performance of these materials. However, it is important to address the high climate impact of NVPF, which emits 22 g CO₂-eq/FU due to the high level of greenhouse gases embodied in its precursor (V_2O_5).

Future research should focus on developing stringent decarbonization-based synthesis strategies for NVP and NVPF HPMs to mitigate their environmental impact. Additionally, further exploration of low-temperature operable cathodes and enhancing the Na⁺ transport kinetics will be crucial for the broader application and commercialization of SIBs. Innovations in cost-effective and environmentally friendly synthesis methods will play a key role in realizing the large-scale practical applications of SIBs, thereby contributing to sustainable energy storage solutions.

Author Contributions: Conceptualization, investigation, methodology, data curation, writing—original draft preparation, K.A. and S.R.; visualization, software, A.B.; validation, formal analysis, S.D.; writing—review and editing, L.F.; supervision, project administration, funding acquisition, T.H.O. All authors have read and agreed to the published version of the manuscript.

Funding: This study was supported by the National Research Foundation of Korea grant funded by the Korean Government (MSIT) (No. 2022R1A2C1004283) and by Korea Basic Science Institute (National research Facilities and Equipment Center) grant funded by the Ministry of Education (2019R1A6C1010046).

Data Availability Statement: Not applicable.

Conflicts of Interest: The authors declare no conflicts of interest.

References

- Ellis, B.L.; Nazar, L.F. Sodium and sodium-ion energy storage batteries. *Curr. Opin. Solid State Mater. Sci.* **2012**, *16*, 168–177. [[CrossRef](#)]
- Pan, H.; Hu, Y.-S.; Chen, L. Room-temperature stationary sodium-ion batteries for large-scale electric energy storage. *Energy Environ. Sci.* **2013**, *6*, 2338–2360. [[CrossRef](#)]
- Delmas, C. Sodium and Sodium-Ion Batteries: 50 Years of Research. *Adv. Energy Mater.* **2018**, *8*, 1703137. [[CrossRef](#)]
- Choi, J.H.; Kim, D.W.; Jung, D.H.; Kim, K.-H.; Kim, J.; Kang, J.K. Low-crystallinity conductive multivalence iron sulfide-embedded S-doped anode and high-surface area O-doped cathode of 3D porous N-rich graphitic carbon frameworks for high-performance sodium-ion hybrid energy storages. *Energy Storage Mater.* **2024**, *68*, 103368. [[CrossRef](#)]
- Hwang, J.-Y.; Myung, S.-T.; Sun, Y.-K. Sodium-ion batteries: Present and future. *Chem. Soc. Rev.* **2017**, *46*, 3529–3614. [[CrossRef](#)]
- Yabuuchi, N.; Kubota, K.; Dahbi, M.; Komaba, S. Research Development on Sodium-Ion Batteries. *Chem. Rev.* **2014**, *114*, 11636–11682. [[CrossRef](#)]
- Zhang, M.; Li, Y.; Wu, F.; Bai, Y.; Wu, C. Boost sodium-ion batteries to commercialization: Strategies to enhance initial Coulombic efficiency of hard carbon anode. *Nano Energy* **2021**, *82*, 105738. [[CrossRef](#)]
- Rui, X.; Zhang, X.; Xu, S.; Tan, H.; Jiang, Y.; Gan, L.Y.; Feng, Y.; Li, C.C.; Yu, Y. A Low-Temperature Sodium-Ion Full Battery: Superb Kinetics and Cycling Stability. *Adv. Funct. Mater.* **2021**, *31*, 2009458. [[CrossRef](#)]
- Abraham, K.M. How Comparable Are Sodium-Ion Batteries to Lithium-Ion Counterparts? *ACS Energy Lett.* **2020**, *5*, 3544–3547. [[CrossRef](#)]
- Li, Y.; Lu, Y.; Zhao, C.; Hu, Y.-S.; Titirici, M.-M.; Li, H.; Huang, X.; Chen, L. Recent advances of electrode materials for low-cost sodium-ion batteries towards practical application for grid energy storage. *Energy Storage Mater.* **2017**, *7*, 130–151. [[CrossRef](#)]
- Rudola, A.; Rennie, A.J.R.; Heap, R.; Meysami, S.S.; Lowbridge, A.; Mazzali, F.; Sayers, R.; Wright, C.J.; Barker, J. Commercialisation of high energy density sodium-ion batteries: Faradion’s journey and outlook. *J. Mater. Chem. A* **2021**, *9*, 8279–8302. [[CrossRef](#)]
- Goikolea, E.; Palomares, V.; Wang, S.; de Larramendi, I.R.; Guo, X.; Wang, G.; Rojo, T. Na-ion batteries—Approaching old and new challenges. *Adv. Energy Mater.* **2020**, *10*, 2002055. [[CrossRef](#)]
- Yadav, P.; Shelke, V.; Patrike, A.; Shelke, M. Sodium-based batteries: Development, commercialization journey and new emerging chemistries. *Oxf. Open Mater. Sci.* **2022**, *3*, itac019. [[CrossRef](#)]
- Barpanda, P.; Nishimura, S.i.; Yamada, A. High-Voltage Pyrophosphate Cathodes. *Adv. Energy Mater.* **2012**, *2*, 841–859. [[CrossRef](#)]
- Masquelier, C.; Croguennec, L. Polyanionic (Phosphates, Silicates, Sulfates) Frameworks as Electrode Materials for Rechargeable Li (or Na) Batteries. *Chem. Rev.* **2013**, *113*, 6552–6591. [[CrossRef](#)]
- Zhang, H.; Gao, Y.; Liu, X.H.; Yang, Z.; He, X.X.; Li, L.; Qiao, Y.; Chen, W.H.; Zeng, R.H.; Wang, Y.; et al. Organic Cathode Materials for Sodium-Ion Batteries: From Fundamental Research to Potential Commercial Application. *Adv. Funct. Mater.* **2022**, *32*, 2107718. [[CrossRef](#)]
- Han, M.H.; Gonzalo, E.; Singh, G.; Rojo, T. A comprehensive review of sodium layered oxides: Powerful cathodes for Na-ion batteries. *Energy Environ. Sci.* **2014**, *8*, 81–102. [[CrossRef](#)]
- Wang, Q.; Xu, J.; Zhang, W.; Mao, M.; Wei, Z.; Wang, L.; Cui, C.; Zhu, Y.; Ma, J. Research progress on vanadium-based cathode materials for sodium ion batteries. *J. Mater. Chem. A* **2018**, *6*, 8815–8838. [[CrossRef](#)]
- Su, D.W.; Dou, S.X.; Wang, G.X. Hierarchical orthorhombic V_2O_5 hollow nanospheres as high performance cathode materials for sodium-ion batteries. *J. Mater. Chem. A* **2014**, *2*, 11185–11194. [[CrossRef](#)]
- Ding, J.; Shen, K.; Du, Z.; Li, B.; Yang, S. 3D-printed hierarchical porous frameworks for sodium storage. *ACS Appl. Mater. Interfaces* **2017**, *9*, 41871–41877. [[CrossRef](#)]
- Yang, X.-Y.; Chen, L.-H.; Li, Y.; Rooke, J.C.; Sanchez, C.; Su, B.-L. Hierarchically porous materials: Synthesis strategies and structure design. *Chem. Soc. Rev.* **2017**, *46*, 481–558. [[CrossRef](#)] [[PubMed](#)]
- Chen, M.; Zhang, Y.; Xing, L.; Liao, Y.; Qiu, Y.; Yang, S.; Li, W. Morphology-Conserved Transformations of Metal-Based Precursors to Hierarchically Porous Micro-/Nanostructures for Electrochemical Energy Conversion and Storage. *Adv. Mater.* **2017**, *29*, 1607015. [[CrossRef](#)] [[PubMed](#)]
- Tang, Y.; Varyambath, A.; Ding, Y.; Chen, B.; Huang, X.; Zhang, Y.; Yu, D.-g.; Kim, I.; Song, W. Porous organic polymers for drug delivery: Hierarchical pore structures, variable morphologies, and biological properties. *Biomater. Sci.* **2022**, *10*, 5369–5390. [[CrossRef](#)] [[PubMed](#)]
- Zhou, X.-L.; Zhang, H.; Shao, L.-M.; Lü, F.; He, P.-J. Preparation and Application of Hierarchical Porous Carbon Materials from Waste and Biomass: A Review. *Waste Biomass Valorization* **2021**, *12*, 1699–1724. [[CrossRef](#)]
- Li, Y.; Fu, Z.Y.; Su, B.L. Hierarchically structured porous materials for energy conversion and storage. *Adv. Funct. Mater.* **2012**, *22*, 4634–4667. [[CrossRef](#)]
- Yao, Q.; Yuan, X.; Chen, T.; Leong, D.T.; Xie, J. Engineering functional metal materials at the atomic level. *Adv. Mater.* **2018**, *30*, 1802751. [[CrossRef](#)] [[PubMed](#)]
- Xi, K.; Cao, S.; Peng, X.; Ducati, C.; Kumar, R.V.; Cheetham, A.K. Carbon with hierarchical pores from carbonized metal–organic frameworks for lithium sulphur batteries. *Chem. Commun.* **2013**, *49*, 2192–2194. [[CrossRef](#)] [[PubMed](#)]
- Yu, L.; Wang, L.P.; Liao, H.; Wang, J.; Feng, Z.; Lev, O.; Loo, J.S.; Sougrati, M.T.; Xu, Z.J. Understanding fundamentals and reaction mechanisms of electrode materials for Na-ion batteries. *Small* **2018**, *14*, 1703338. [[CrossRef](#)] [[PubMed](#)]

29. Liu, P.; Yi, H.; Chen, X.; Zhu, K.; Li, Z.; Sun, Z.; Jiao, L. Hierarchical engineering for high-energy-oriented sodium-ion batteries. *Acc. Mater. Res.* **2022**, *3*, 672–684. [[CrossRef](#)]
30. Zhu, Q.; Chang, X.; Sun, N.; Chen, R.; Zhao, Y.; Xu, B.; Wu, F. Confined growth of nano-Na₃V₂(PO₄)₃ in porous carbon framework for high-rate Na-ion storage. *ACS Appl. Mater. Interfaces* **2018**, *11*, 3107–3115. [[CrossRef](#)]
31. Zhang, X.; Rui, X.; Chen, D.; Tan, H.; Yang, D.; Huang, S.; Yu, Y. Na₃V₂(PO₄)₃: An advanced cathode for sodium-ion batteries. *Nanoscale* **2019**, *11*, 2556–2576. [[CrossRef](#)] [[PubMed](#)]
32. Chen, S.; Wu, C.; Shen, L.; Zhu, C.; Huang, Y.; Xi, K.; Maier, J.; Yu, Y. Challenges and perspectives for NASICON-type electrode materials for advanced sodium-ion batteries. *Adv. Mater.* **2017**, *29*, 1700431. [[CrossRef](#)] [[PubMed](#)]
33. Parashar, M.; Shukla, V.K.; Singh, R. Metal oxides nanoparticles via sol–gel method: A review on synthesis, characterization and applications. *J. Mater. Sci. Mater. Electron.* **2020**, *31*, 3729–3749. [[CrossRef](#)]
34. Navas, D.; Fuentes, S.; Castro-Alvarez, A.; Chavez-Angel, E. Review on sol-gel synthesis of perovskite and oxide nanomaterials. *Gels* **2021**, *7*, 275. [[CrossRef](#)] [[PubMed](#)]
35. Li, Y.; Zhu, J.; Cheng, H.; Li, G.; Cho, H.; Jiang, M.; Gao, Q.; Zhang, X. Developments of advanced electrospinning techniques: A critical review. *Adv. Mater. Technol.* **2021**, *6*, 2100410. [[CrossRef](#)]
36. Aruchamy, K.; Mahto, A.; Nataraj, S. Electrospun nanofibers, nanocomposites and characterization of art: Insight on establishing fibers as product. *Nano-Struct. Nano-Objects* **2018**, *16*, 45–58. [[CrossRef](#)]
37. Xue, J.; Wu, T.; Dai, Y.; Xia, Y. Electrospinning and electrospun nanofibers: Methods, materials, and applications. *Chem. Rev.* **2019**, *119*, 5298–5415. [[CrossRef](#)] [[PubMed](#)]
38. Rui, X.; Sun, W.; Wu, C.; Yu, Y.; Yan, Q. An Advanced Sodium-Ion Battery Composed of Carbon Coated Na₃V₂(PO₄)₃ in a Porous Graphene Network. *Adv. Mater.* **2015**, *27*, 6670–6676. [[CrossRef](#)] [[PubMed](#)]
39. Ni, Q.; Bai, Y.; Li, Y.; Ling, L.; Li, L.; Chen, G.; Wang, Z.; Ren, H.; Wu, F.; Wu, C. 3D Electronic Channels Wrapped Large-Sized Na₃V₂(PO₄)₃ as Flexible Electrode for Sodium-Ion Batteries. *Small* **2018**, *14*, e1702864. [[CrossRef](#)]
40. Tian, Z.; Chen, Y.; Sun, S.; Liu, H.; Wang, C.; Huang, Q.; Liu, C.; Wang, Y.; Guo, L. Constructing hierarchical heterojunction structure for K/Co co-substituted Na₃V₂(PO₄)₃ by integrating carbon quantum dots. *J. Colloid Interface Sci.* **2022**, *613*, 536–546. [[CrossRef](#)]
41. Wang, Z.; Han, J.; Wang, D.; Liu, L.; Shi, W.; Xiong, F.; Tao, H. Pore-forming mechanisms and sodium-ion-storage performances in a porous Na₃V₂(PO₄)₃/C composite cathode. *Dalton Trans.* **2023**, *52*, 4708–4716. [[CrossRef](#)]
42. Byrappa, K.; Yoshimura, M. *Handbook of Hydrothermal Technology*, 2nd ed.; William Andrew: Norwich, NY, USA, 2013; pp. 51–73. [[CrossRef](#)]
43. Aruchamy, K.; Nagaraj, R.; Manohara, H.M.; Nidhi, M.R.; Mondal, D.; Ghosh, D.; Nataraj, S.K. One-step green route synthesis of spinel ZnMn₂O₄ nanoparticles decorated on MWCNTs as a novel electrode material for supercapacitor. *Mater. Sci. Eng. B* **2020**, *252*, 114481. [[CrossRef](#)]
44. Aruchamy, K.; Balasankar, A.; Ramasundaram, S.; Oh, T.H. Recent design and synthesis strategies for high-performance supercapacitors utilizing ZnCo₂O₄-based electrode materials. *Energies* **2023**, *16*, 5604. [[CrossRef](#)]
45. Kang, S.; Wang, C.; Chen, J.; Meng, T.; Jiaqiang, E. Progress on solvo/hydrothermal synthesis and optimization of the cathode materials of lithium-ion battery. *J. Energy Storage* **2023**, *67*, 107515. [[CrossRef](#)]
46. Ruan, Y.; Liu, J.; Song, S.; Jiang, N.; Battaglia, V. Multi-hierarchical nanosheet-assembled chrysanthemum-structured Na₃V₂(PO₄)₃/C as electrode materials for high-performance sodium-ion batteries. *Ionics* **2018**, *24*, 1663–1673. [[CrossRef](#)]
47. Li, H.; Bi, X.; Bai, Y.; Yuan, Y.; Shahbazian-Yassar, R.; Wu, C.; Wu, F.; Lu, J.; Amine, K. High-Rate, Durable Sodium-Ion Battery Cathode Enabled by Carbon-Coated Micro-Sized Na₃V₂(PO₄)₃ Particles with Interconnected Vertical Nanowalls. *Adv. Mater. Interfaces* **2016**, *3*, 1500740. [[CrossRef](#)]
48. Ling, R.; Cai, S.; Xie, D.; Li, X.; Wang, M.; Lin, Y.; Jiang, S.; Shen, K.; Xiong, K.; Sun, X. Three-dimensional hierarchical porous Na₃V₂(PO₄)₃/C structure with high rate capability and cycling stability for sodium-ion batteries. *Chem. Eng. J.* **2018**, *353*, 264–272. [[CrossRef](#)]
49. Cao, X.; Pan, A.; Yin, B.; Fang, G.; Wang, Y.; Kong, X.; Zhu, T.; Zhou, J.; Cao, G.; Liang, S. Nanoflake-constructed porous Na₃V₂(PO₄)₃/C hierarchical microspheres as a bicontinuous cathode for sodium-ion batteries applications. *Nano Energy* **2019**, *60*, 312–323. [[CrossRef](#)]
50. Chen, H.; Yang, Y.; Nie, R.; Li, C.; Xu, S.; Zhou, M.; Zhang, X.; Zhou, H. Micro-nano Na₃V₂(PO₄)₃/C derived from metal-organic frameworks for high performance sodium ion batteries. *J. Alloys Compd.* **2023**, *932*, 167695. [[CrossRef](#)]
51. Zheng, W.; Gao, R.; Zhou, T.; Huang, X. Enhanced electrochemical performance of Na₃V₂(PO₄)₃ with Ni²⁺ doping by a spray drying-assisted process for sodium ion batteries. *Solid State Ion.* **2018**, *324*, 183–190. [[CrossRef](#)]
52. Zheng, L.-L.; Xue, Y.; Liu, B.-S.; Zhou, Y.-X.; Hao, S.-E.; Wang, Z.-b. High performance Na₃V₂(PO₄)₃ cathode prepared by a facile solution evaporation method for sodium-ion batteries. *Ceram. Int.* **2017**, *43*, 4950–4956. [[CrossRef](#)]
53. Zheng, W.; Huang, X.; Ren, Y.; Wang, H.; Zhou, S.; Chen, Y.; Ding, X.; Zhou, T. Porous spherical Na₃V₂(PO₄)₃/C composites synthesized via a spray drying-assisted process with high-rate performance as cathode materials for sodium-ion batteries. *Solid State Ion.* **2017**, *308*, 161–166. [[CrossRef](#)]
54. Saravanan, K.; Mason, C.W.; Rudola, A.; Wong, K.H.; Balaya, P. The First Report on Excellent Cycling Stability and Superior Rate Capability of Na₃V₂(PO₄)₃ for Sodium Ion Batteries. *Adv. Energy Mater.* **2013**, *3*, 444–450. [[CrossRef](#)]

55. Wei, T.; Yang, G.; Wang, C. Bottom-up assembly of strongly-coupled $\text{Na}_3\text{V}_2(\text{PO}_4)_3/\text{C}$ into hierarchically porous hollow nanospheres for high-rate and -stable Na-ion storage. *Nano Energy* **2017**, *39*, 363–370. [[CrossRef](#)]
56. Salehi, A.H.; Masoudpanah, S.M.; Hasheminiasari, M.; Yaghtin, A.; Safanama, D.; Ong, C.K.; Adams, S.; Zaghib, K.; Reddy, M.V. Facile synthesis of hierarchical porous $\text{Na}_3\text{V}_2(\text{PO}_4)_3/\text{C}$ composites with high-performance Na storage properties. *J. Power Sources* **2021**, *481*, 228828. [[CrossRef](#)]
57. Xiong, H.; Sun, G.; Liu, Z.; Zhang, L.; Li, L.; Zhang, W.; Du, F.; Qiao, Z.A. Polymer Stabilized Droplet Templating towards Tunable Hierarchical Porosity in Single Crystalline $\text{Na}_3\text{V}_2(\text{PO}_4)_3$ for Enhanced Sodium-Ion Storage. *Angew. Chem. Int. Ed.* **2021**, *60*, 10334–10341. [[CrossRef](#)]
58. Li, L.; Xu, Y.; Sun, X.; Chang, R.; Zhang, Y.; Zhang, X.; Li, J. Fluorophosphates from solid-state synthesis and electrochemical ion exchange: NaVPO_4F or $\text{Na}_3\text{V}_2(\text{PO}_4)_2\text{F}_3$? *Adv. Energy Mater.* **2018**, *8*, 1801064. [[CrossRef](#)]
59. Van Nghia, N.; Jafian, S.; Hung, I.-M. Synthesis and electrochemical performance of the $\text{Na}_3\text{V}_2(\text{PO}_4)_3$ cathode for sodium-ion batteries. *J. Electron. Mater.* **2016**, *45*, 2582–2590. [[CrossRef](#)]
60. Semykina, D.O.; Sharafutdinov, M.R.; Kosova, N.V. Understanding of the Mechanism and Kinetics of the Fast Solid-State Reaction between NaF and VPO_4 to Form $\text{Na}_3\text{V}_2(\text{PO}_4)_2\text{F}_3$. *Inorg. Chem.* **2022**, *61*, 10023–10035. [[CrossRef](#)]
61. Liu, X.; Feng, G.; Wu, Z.; Wang, D.; Wu, C.; Yang, L.; Xiang, W.; Chen, Y.; Guo, X.; Zhong, B. Investigating the influence of sodium sources towards improved $\text{Na}_3\text{V}_2(\text{PO}_4)_3$ cathode of sodium-ion batteries. *J. Alloys Compd.* **2020**, *815*, 152430. [[CrossRef](#)]
62. Fang, Y.; Xiao, L.; Ai, X.; Cao, Y.; Yang, H. Hierarchical Carbon Framework Wrapped $\text{Na}_3\text{V}_2(\text{PO}_4)_3$ as a Superior High-Rate and Extended Lifespan Cathode for Sodium-Ion Batteries. *Adv. Mater.* **2015**, *27*, 5895–5900. [[CrossRef](#)] [[PubMed](#)]
63. Liang, X.; Ou, X.; Zheng, F.; Pan, Q.; Xiong, X.; Hu, R.; Yang, C.; Liu, M. Surface Modification of $\text{Na}_3\text{V}_2(\text{PO}_4)_3$ by Nitrogen and Sulfur Dual-Doped Carbon Layer with Advanced Sodium Storage Property. *ACS Appl. Mater. Interfaces* **2017**, *9*, 13151–13162. [[CrossRef](#)] [[PubMed](#)]
64. Li, J.; Cao, X.; Pan, A.; Zhao, Y.; Yang, H.; Cao, G.; Liang, S. Nanoflake-assembled three-dimensional $\text{Na}_3\text{V}_2(\text{PO}_4)_3/\text{C}$ cathode for high performance sodium ion batteries. *Chem. Eng. J.* **2018**, *335*, 301–308. [[CrossRef](#)]
65. Zhao, Y.; Cao, X.; Fang, G.; Wang, Y.; Yang, H.; Liang, S.; Pan, A.; Cao, G. Hierarchically carbon-coated $\text{Na}_3\text{V}_2(\text{PO}_4)_3$ nanoflakes for high-rate capability and ultralong cycle-life sodium ion batteries. *Chem. Eng. J.* **2018**, *339*, 162–169. [[CrossRef](#)]
66. Xu, S.; Yao, K.; Yang, D.; Chen, D.; Lin, C.; Liu, C.; Wu, H.; Zeng, J.; Liu, L.; Zheng, Y.; et al. Interfacial Engineering of $\text{Na}_3\text{V}_2(\text{PO}_4)_2\text{O}_2\text{F}$ Cathode for Low-Temperature (-40°C) Sodium-Ion Batteries. *ACS Appl. Mater. Interfaces* **2023**, *15*, 14329–14338. [[CrossRef](#)]
67. Xu, S.; Yang, Y.; Tang, F.; Yao, Y.; Lv, X.; Liu, L.; Xu, C.; Feng, Y.; Rui, X.; Yu, Y. Vanadium fluorophosphates: Advanced cathode materials for next-generation secondary batteries. *Mater. Horiz.* **2023**, *10*, 1901–1923. [[CrossRef](#)] [[PubMed](#)]
68. Serras, P.; Palomares, V.; Goñi, A.; Muro, I.G.d.; Kubiak, P.; Lezama, L.; Rojo, T. High voltage cathode materials for Na-ion batteries of general formula $\text{Na}_3\text{V}_2\text{O}_{2x}(\text{PO}_4)_2\text{F}_{3-2x}$. *J. Mater. Chem.* **2012**, *22*, 22301–22308. [[CrossRef](#)]
69. Serras, P.; Palomares, V.; Alonso, J.; Sharma, N.; López del Amo, J.M.; Kubiak, P.; Fdez-Gubieda, M.L.; Rojo, T. Electrochemical Na Extraction/Insertion of $\text{Na}_3\text{V}_2\text{O}_{2x}(\text{PO}_4)_2\text{F}_{3-2x}$. *Chem. Mater.* **2013**, *25*, 4917–4925. [[CrossRef](#)]
70. Kumar, P.R.; Jung, Y.H.; Lim, C.H.; Kim, D.K. $\text{Na}_3\text{V}_2\text{O}_{2x}(\text{PO}_4)_2\text{F}_{3-2x}$: A stable and high-voltage cathode material for aqueous sodium-ion batteries with high energy density. *J. Mater. Chem. A* **2015**, *3*, 6271–6275. [[CrossRef](#)]
71. Jin, H.; Dong, J.; Uchaker, E.; Zhang, Q.; Zhou, X.; Hou, S.; Li, J.; Cao, G. Three dimensional architecture of carbon wrapped multilayer $\text{Na}_3\text{V}_2\text{O}_2(\text{PO}_4)_2\text{F}$ nanocubes embedded in graphene for improved sodium ion batteries. *J. Mater. Chem. A* **2015**, *3*, 17563–17568. [[CrossRef](#)]
72. Guo, J.Z.; Wang, P.F.; Wu, X.L.; Zhang, X.H.; Yan, Q.; Chen, H.; Zhang, J.P.; Guo, Y.G. High-Energy/Power and Low-Temperature Cathode for Sodium-Ion Batteries: In Situ XRD Study and Superior Full-Cell Performance. *Adv. Mater.* **2017**, *29*, 1701968. [[CrossRef](#)] [[PubMed](#)]
73. Zhu, C.; Wu, C.; Chen, C.-C.; Kopold, P.; Aken, P.A.v.; Maier, J.; Yu, Y. A High Power-High Energy $\text{Na}_3\text{V}_2(\text{PO}_4)_2\text{F}_3$ Sodium Cathode: Investigation of Transport Parameters, Rational Design and Realization. *Chem. Mater.* **2017**, *29*, 5207–5215. [[CrossRef](#)]
74. Aruchamy, K.; Bisht, M.; Venkatesu, P.; Kalpana, D.; Nidhi, M.; Singh, N.; Ghosh, D.; Mondal, D.; Nataraj, S.K. Direct conversion of lignocellulosic biomass to biomimetic tendril-like functional carbon helices: A protein friendly host for cytochrome C. *Green Chem.* **2018**, *20*, 3711–3716. [[CrossRef](#)]
75. Chakraborty, S.; Aruchamy, K.; Ghosh, D.; Singh, N.; Prasad, K.; Kalpana, D.; Nataraj, S.; Mondal, D. Engineering Fe-doped highly oxygenated solvothermal carbon from glucose-based eutectic system as active microcleaner and efficient carbocatalyst. *J. Mater. Chem. A* **2019**, *7*, 4988–4997.
76. Manohara, H.M.; Aruchamy, K.; Chakraborty, S.; Radha, N.; Nidhi, M.R.; Ghosh, D.; Nataraj, S.K.; Mondal, D. Sustainable water purification using an engineered solvothermal carbon based membrane derived from a eutectic system. *ACS Sustain. Chem. Eng.* **2019**, *7*, 10143–10153. [[CrossRef](#)]
77. Feng, S.-H.; Li, G.-H. Hydrothermal and solvothermal syntheses. In *Modern Inorganic Synthetic Chemistry*; Elsevier: Amsterdam, The Netherlands, 2017; pp. 73–104.
78. Xu, M.; Wang, L.; Zhao, X.; Song, J.; Xie, H.; Lu, Y.; Goodenough, J.B. $\text{Na}_3\text{V}_2\text{O}_2(\text{PO}_4)_2\text{F}/\text{graphene}$ sandwich structure for high-performance cathode of a sodium-ion battery. *Phys. Chem. Chem. Phys.* **2013**, *15*, 13032–13037. [[CrossRef](#)] [[PubMed](#)]

79. Qi, Y.; Mu, L.; Zhao, J.; Hu, Y.S.; Liu, H.; Dai, S. Superior Na-Storage Performance of Low-Temperature-Synthesized $\text{Na}_3(\text{VO}_{1-x}\text{PO}_4)_2\text{F}_{1+2x}$ ($0 \leq x \leq 1$) Nanoparticles for Na-Ion Batteries. *Angew. Chem. Int. Ed.* **2015**, *54*, 9911–9916. [CrossRef] [PubMed]
80. Deng, G.; Chao, D.; Guo, Y.; Chen, Z.; Wang, H.; Savilov, S.V.; Lin, J.; Shen, Z.X. Graphene quantum dots-shielded $\text{Na}_3(\text{VO})_2(\text{PO}_4)_2\text{F}@\text{C}$ nanocuboids as robust cathode for Na-ion battery. *Energy Storage Mater.* **2016**, *5*, 198–204. [CrossRef]
81. Jin, H.; Liu, M.; Uchaker, E.; Dong, J.; Zhang, Q.; Hou, S.; Li, J.; Cao, G. Nanoporous carbon leading to the high performance of a $\text{Na}_3\text{V}_2\text{O}_2(\text{PO}_4)_2\text{F}@\text{carbon}/\text{graphene}$ cathode in a sodium ion battery. *CrystEngComm* **2017**, *19*, 4287–4293. [CrossRef]
82. Chao, D.; Lai, C.H.; Liang, P.; Wei, Q.; Wang, Y.S.; Zhu, C.; Deng, G.; Doan-Nguyen, V.V.T.; Lin, J.; Mai, L.; et al. Sodium Vanadium Fluorophosphates (NVOPF) Array Cathode Designed for High-Rate Full Sodium Ion Storage Device. *Adv. Energy Mater.* **2018**, *8*, 1800058. [CrossRef]
83. Zhao, L.; Rong, X.; Niu, Y.; Xu, R.; Zhang, T.; Li, T.; Yu, Y.; Hou, Y. Ostwald Ripening Tailoring Hierarchically Porous $\text{Na}_3\text{V}_2(\text{PO}_4)_2\text{O}_2\text{F}$ Hollow Nanospheres for Superior High-Rate and Ultrastable Sodium Ion Storage. *Small* **2020**, *16*, e2004925. [CrossRef] [PubMed]
84. Liu, S.; Cao, X.; Zhang, Y.; Wang, K.; Su, Q.; Chen, J.; He, Q.; Liang, S.; Cao, G.; Pan, A. Carbon quantum dot modified $\text{Na}_3\text{V}_2(\text{PO}_4)_2\text{F}_3$ as a high-performance cathode material for sodium-ion batteries. *J. Mater. Chem. A* **2020**, *8*, 18872–18879. [CrossRef]
85. Du, P.; Mi, K.; Hu, F.; Jiang, X.; Wang, D.; Zheng, X. Hierarchical hollow microspheres $\text{Na}_3\text{V}_2(\text{PO}_4)_2\text{F}_3\text{C}@\text{rGO}$ as high-performance cathode materials for sodium ion batteries. *New J. Chem.* **2020**, *44*, 12985–12992. [CrossRef]
86. Liang, K.; Wang, S.; Zhao, H.; Huang, X.; Ren, Y.; He, Z.; Mao, J.; Zheng, J. A facile strategy for developing uniform hierarchical $\text{Na}_3\text{V}_2(\text{PO}_4)_2\text{F}_3@\text{carbonized polyacrylonitrile}$ multi-clustered hollow microspheres for high-energy-density sodium-ion batteries. *Chem. Eng. J.* **2022**, *428*, 131780. [CrossRef]
87. Yin, Y.; Xiong, F.; Pei, C.; Xu, Y.; An, Q.; Tan, S.; Zhuang, Z.; Sheng, J.; Li, Q.; Mai, L. Robust three-dimensional graphene skeleton encapsulated $\text{Na}_3\text{V}_2\text{O}_2(\text{PO}_4)_2\text{F}$ nanoparticles as a high-rate and long-life cathode of sodium-ion batteries. *Nano Energy* **2017**, *41*, 452–459. [CrossRef]
88. Langrock, A.; Xu, Y.; Liu, Y.; Ehrman, S.; Manivannan, A.; Wang, C. Carbon coated hollow $\text{Na}_2\text{FePO}_4\text{F}$ spheres for Na-ion battery cathodes. *J. Power Sources* **2013**, *223*, 62–67. [CrossRef]
89. Kawabe, Y.; Yabuuchi, N.; Kajiyama, M.; Fukuhara, N.; Inamasu, T.; Okuyama, R.; Nakai, I.; Komaba, S. Synthesis and electrode performance of carbon coated $\text{Na}_2\text{FePO}_4\text{F}$ for rechargeable Na batteries. *Electrochim. Commun.* **2011**, *13*, 1225–1228. [CrossRef]
90. Park, Y.U.; Seo, D.H.; Kim, H.; Kim, J.; Lee, S.; Kim, B.; Kang, K. A Family of High-Performance Cathode Materials for Na-ion Batteries, $\text{Na}_3(\text{VO}_{1-x}\text{PO}_4)_2\text{F}_{1+2x}$ ($0 \leq x \leq 1$): Combined First-Principles and Experimental Study. *Adv. Funct. Mater.* **2014**, *24*, 4603–4614. [CrossRef]
91. Deng, X.; Shi, W.; Sunarso, J.; Liu, M.; Shao, Z. A Green Route to a $\text{Na}_2\text{FePO}_4\text{F}$ -Based Cathode for Sodium Ion Batteries of High Rate and Long Cycling Life. *ACS Appl. Mater. Interfaces* **2017**, *9*, 16280–16287. [CrossRef]
92. Hou, Y.; Chang, K.; Wang, Z.; Gu, S.; Liu, Q.; Zhang, J.; Cheng, H.; Zhang, S.; Chang, Z.; Lu, Z. Rapid microwave-assisted refluxing synthesis of hierarchical mulberry-shaped $\text{Na}_3\text{V}_2(\text{PO}_4)_2\text{O}_2\text{F}@\text{C}$ as high performance cathode for sodium & lithium-ion batteries. *Sci. China Mater.* **2019**, *62*, 474–486. [CrossRef]
93. He, J.; Tao, T.; Yang, F.; Sun, Z.; Huang, H. Phase-manipulated hierarchically core-shell $\text{Na}_3(\text{VO}_{1-x}\text{PO}_4)_2\text{F}_{1+2x}$ ($0 \leq x \leq 1$)@ $\text{Na}_3\text{V}_2(\text{PO}_4)_3$ and its synergistic effect with conformally wrapped reduced graphene oxide framework towards high-performance cathode for sodium-ion batteries. *Mater. Today Phys.* **2022**, *27*, 100813. [CrossRef]
94. Zhang, X.; Zhang, Z.; Xu, S.; Xu, C.; Rui, X. Advanced Vanadium Oxides for Sodium-Ion Batteries. *Adv. Funct. Mater.* **2023**, *33*, 2306055. [CrossRef]
95. Zhao, Z.; Li, D.; Wang, C.; Fang, D.; Wang, B.; Li, J.; Jin, H. Hierarchical V_2O_5 microspheres: A pseudocapacitive cathode material for enhanced sodium ion storage. *J. Alloys Compd.* **2022**, *895*, 162617. [CrossRef]
96. Tang, R.; Li, K.; Liu, C.; Liu, Y.; Gong, Y.; Lin, J. Long-lifespan benzoquinone-intercalated vanadium oxide with vacancies and disorders on the (00l) facets for efficient sodium-ion battery: A facile approach to Na^+ capture and pre-sodiation. *Chem. Eng. J.* **2023**, *453*, 139734. [CrossRef]

Disclaimer/Publisher's Note: The statements, opinions and data contained in all publications are solely those of the individual author(s) and contributor(s) and not of MDPI and/or the editor(s). MDPI and/or the editor(s) disclaim responsibility for any injury to people or property resulting from any ideas, methods, instructions or products referred to in the content.